

Article

New Insights into the Genesis of Dibrova U-Th-REE Mineral Deposit (West Azov Megablock, Ukraine) Using Monazite Chemistry

Kateryna Poliakovska ^{1,2,*} , Volodymyr Pokalyuk ³ , Irvine R. Annesley ^{2,4} and Olena Ivanik ^{1,5}

¹ Institute of Geology, Taras Shevchenko National University of Kyiv, 60 Volodymyrska Street, 01033 Kyiv, Ukraine; om.ivanik@gmail.com

² Université de Lorraine, CNRS, GeoRessources, Campus Aiguillettes, rue Jacques Callot BP 70239, 54506 Vandœuvre-lès-Nancy, France; jnrirvine@gmail.com

³ The Institute of Environmental Geochemistry of National Academy of Sciences of Ukraine, 03142 Kyiv, Ukraine; pvskan@ukr.net

⁴ Department of Geological Sciences, University of Saskatchewan, 114 Science Place, Saskatoon, SK S7N5E2, Canada

⁵ Centre de Recherches Pétrographiques et Géochimiques (CRPG), UMR 7358 CNRS-UL, 15 Rue Notre Dame des Pauvres, 54500 Vandœuvre-lès-Nancy, France

* Correspondence: kateryna.poliakovska@gmail.com

Abstract: This paper investigates the monazite grains from the Dibrova rare-earth-thorium-uranium (U-Th-REE) mineral deposit within the Azov Megablock of Ukrainian Shield. U-Th-REE mineralization is associated with K-feldspar-quartz metasandstones and metagritstones (hereafter quartzites) and pegmatoids. The latter possibly represent products of ultrametamorphism/granitization of initially sedimentary clastic rocks during tectono-magmatic activation during the Paleoproterozoic. Ores are composed of quartz as a principal mineral, feldspar, sillimanite, muscovite, monazite, brannerite, uraninite, zircon, rutile, and sulfides. The purpose of this work was to obtain insights into the genesis of the mineral deposit by studying the monazite grains, their chemistry, and ages. Petrographic research work was carried out that included studying/analyzing the monazites from various monazite-bearing rocks (quartzites, pegmatoid, and biotite schist samples). A variety of methods and tools were used, including optical microscopy study, X-ray fluorescence (XRF) mapping of selected samples, as well as scanning electron microscope (SEM) and electron microprobe (EPMA) characterization of monazites, including U-Th-Pb monazite chemical dating. U-Pb-Th chemical electron microprobe dating of the monazites yielded two major distinct monazite age groups at 3.0–2.8 Ga and 2.2–2.0 Ga. The first age group corresponds to the time of formation of the Archean granitoids, which served as a source of monazite for its clastic sedimentation during the Paleoproterozoic in the Dibrova suite sediments. The second age group corresponds to the reprecipitation (i.e., remobilization) of monazite during the Paleoproterozoic tectono-magmatic activation. The location of the mineral deposit within the deep mantle-crustal Devladiivska shear zone is another favorable factor for the remobilization and transport of metals. New data on the age of mineralization yield a more complete understanding of the geological history and formation of the complex polyphase rare-earth-uranium-thorium Dibrova mineral deposit.

Keywords: monazite; uranium; thorium; rare-earth elements; Ukrainian Shield; Dibrova mineral deposit; metamorphic processes



Citation: Poliakovska, K.; Pokalyuk, V.; Annesley, I.R.; Ivanik, O. New Insights into the Genesis of Dibrova U-Th-REE Mineral Deposit (West Azov Megablock, Ukraine) Using Monazite Chemistry. *Minerals* **2023**, *13*, 1241. <https://doi.org/10.3390/min13101241>

Academic Editors: Bernhard Schulz, Jaroslav Dostal, Maria Economou-Eliopoulos, Martiya Sadeghi and David Lentz

Received: 3 August 2023

Revised: 20 September 2023

Accepted: 21 September 2023

Published: 23 September 2023



Copyright: © 2023 by the authors. Licensee MDPI, Basel, Switzerland. This article is an open access article distributed under the terms and conditions of the Creative Commons Attribution (CC BY) license (<https://creativecommons.org/licenses/by/4.0/>).

1. Introduction

The Ukrainian Shield is prospective for rare-earth deposits and occurrences. Most igneous deposits and the majority of occurrences of rare metals are genetically linked to Paleoproterozoic intrusive complexes, which formed between 1.7 and 2.1 billion years ago [1,2]. These complexes consist of alkaline and subalkaline rocks, carbonatites, and

granitic pegmatites. In some cases, they are also associated with metasomatic rocks that accompany the ore-bearing igneous formations, although to a lesser extent [2]. Acquiring a comprehensive understanding of rare-metals mineral systems is a fundamental component in identifying new prospects and effectively addressing supply shortages that arise due to the increasing global demand [3–6].

In our study, we investigated the Dibrova mineral deposit of complex uranium-thorium-rare-earth ore within the Azov Megablock of Ukrainian Shield. The Dibrova (Dibrovské) mineral deposit (approximate coordinates: 48°03′54.0″ N 36°29′24.0″ E) was discovered during geological mapping at a scale of 1:50,000 from 1984 to 1988. The mineral deposit is located within the junction zone of the northwestern part of the West Azov Megablock with the Dnieper-Donets depression (Figure 1) [7]. The rare-earth elements (REE), thorium (Th), and uranium (U) are hosted mostly in monazite, brannerite, and uraninite, that are associated with metamorphically altered (by dislocation metamorphism) K-feldspar-quartz metasedimentary quartzites (hereafter called quartzites) and pegmatoids. The genesis of pegmatoids is still unclear: they are either altered (blastocataclastic) intrusive veins within quartzites, or they are a product of granitization of the original clastic sediments rich in potassium and alumina.

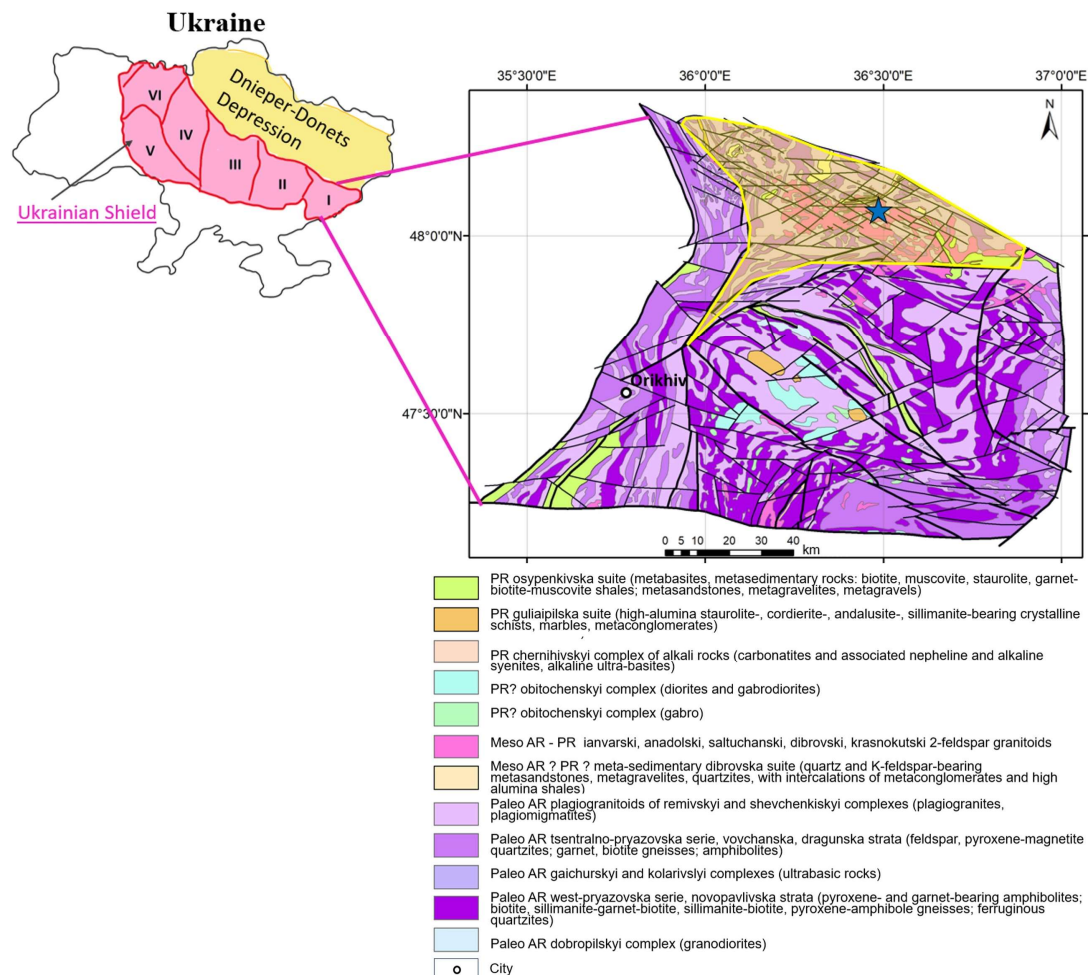


Figure 1. Regional position of Dibrova mineral deposit within the Ukrainian Shield. Schematic contours of Ukraine (left) with the Ukrainian Shield scheme (in magenta). Numbers represent the megablocks of the Ukrainian Shield: I—Azov Megablock, II—Middle-Dnipro Megablock, III—Kirovohrad Megablock; IV—Ros-Tykych Megablock; V—Podilsky Megablock; VI—Volyn Megablock. Blow-up figure shows the geology of the West Azov Megablock in details (modified from [8]); the zone in transparent yellow shows the extends of Vovchansky Block (modified from [8]). Blue star marks the location of Dibrova mineral deposit. Abbreviations: AR = Archean; PR = Proterozoic.

Several hypotheses have been suggested for the Dibrova mineralization genesis:

1. Sedimentary-metamorphosed mineralization [7,9];
2. Sedimentary-metamorphic mineralization regenerated in a deep fault zone [10–12];
3. Post-magmatic, metasomatic, pneumatolithic—hydrothermal mineralization, associated with potassic granites [8,13];
4. Deep-fluidized mineralization—polygenic, polychronous mineralization with participation of transcrustal mantle fluids [14];
5. Tectono-metamorphic remobilization, formed in the process of multistage tectono-metamorphic transformation of the Archean-Paleoproterozoic crystalline substrate in the shear dislocation system and localized in places of lower pressure—“pressure shadows” [15].

Kichurchak et al. [7], who first discovered the Dibrova mineralization, suggested the primary sedimentary (paleoplacer/paleo quartz-pebble conglomerates type) hypothesis to explain the genesis of the mineral deposit. Several tectono-metamorphic models [9–12] are also based on the concepts of primacy of sedimentary genesis of mineralization, which was further enriched during remobilization and new precipitation of ore minerals. At the moment, it remains the dominant hypothesis. Another group of experts consider an exclusively hydrothermal-metasomatic origin of mineralization [8,13], associated with magmatic and post-magmatic stages and intrusion of Mesoarchean aplite-pegmatoid granites. In [14], based on theoretical generalizations, another hypothesis was presented that suggested a mantle source of ore material, which was transported to the upper crustal horizons by fluids and metasomatic processes using the Devladvivska fault zone as a pathway.

The general characteristics of this mineral deposit were highlighted in the following research work: [7–9,13,14,16–18]. However, the genesis and age of the complex U-Th-REE mineralization have not yet been sufficiently researched. Thus, in our paper we try to establish which hypothesis is correct. In this work, we provide a brief overview of the Dibrova mineralized area and study in much more detail the U-Th-REE mineralization of monazite and associated minerals to answer some of the outstanding metallogenetic questions. Petrographic study has been carried out to document the characteristics of the Dibrova mineralization, in particular by studying the monazites from various monazite-bearing rocks (from quartzite, pegmatoid, and biotite schist samples).

A variety of methods and tools were used, including optical microscopy study, X-ray fluorescence (XRF) mapping of selected samples, as well as scanning electron microscope (SEM) and electron microprobe (EPMA) characterization of monazites including U-Th-Pb monazite chemical dating. New data on the age of mineralization were obtained which yield a more complete understanding of the geological history and formation of the Dibrova mineral deposit.

2. Regional Geological Setting

The West Azov area is a constituent part of the Azov (Priazovsky) Megablock (granulite-greenstone type) and occupies the extreme eastern part the Ukrainian Shield. The region primarily consists of Archean and Paleoproterozoic rocks, prominently including granitoids and metamorphic rocks such as gneisses, schists, and amphibolites. The western limit of the Azov Megablock is the Orikhov-Pavlograd deep fault, or the much larger Orikhov-Pavlograd fault zone [19].

On a regional scale, the following principal thermo-tectonic events that reflect the general evolution of the region's development during the Precambrian have been identified. The Meso- and Neo-Archean (3.0–2.6 Ga) were characterized by the formation of greenstone belts and plagiogranitoid massifs; the Paleoproterozoic (2.5–2.3 Ga) by the formation of sedimentary complexes, including ferruginous-siliceous formations. The 2.1–2.0 Ga time period was characterized by tectonic-magmatic activity, accompanied by regional

metamorphism and deep folding with extensive potassium-type granitization, and at 1.7 Ga the formation of polyphase plutons (e.g., sienites, granosienites) [19,20].

The megablock is considered to be a fragment of the Archean granite-greenstone area/craton involved in collisional Paleoproterozoic metamorphism. The structure of the Azov Megablock is dominated by Mesoproterozoic granitic-gneiss domes and the surrounding synforms and monoclines. In the interdome areas, highly deformed and high-grade metamorphic supracrustal rock complexes are observed. The megablock is characterized by significant intensity and unevenness of metamorphism, ranging from epidote-amphibolite to granulite facies [9].

The U-Th-REE Dibrova mineral deposit is located within the northern part of the Vovchansky tectonic block (Figures 1 and 2). The Vovchansky tectonic block is a component of the Azov Megablock, which is recognized as a rare-metal-rare-earth subprovince within the extensive rare-metal province of the Ukrainian Shield [8]. The structural configuration of the Vovchansky tectonic block is characterized by a fold-dome structure composed of two levels, primarily consisting of antiformal structures (Figure 2, Table 1). The lower level comprises Paleo-Archean metamorphic rocks of Remivskyi complex (plagiogranitoids), that underwent remobilization during the late Meso-Archean period (Shevchenkiv stage of ultrametamorphism). Smaller amphibolite and gneiss bodies are also present within these rocks, forming predominantly domed antiformal structures. The upper-level rocks, which are co-folded together with the lower Paleoproterozoic structural layer, are separated from the lower level by a stratigraphic unconformity. This upper structural level encompasses metamorphosed (amphibolite-granulite facies conditions) volcanic and sedimentary rocks. It also includes two-feldspar granites from the Janvarskyi complex and Paleoproterozoic granitoids from several complexes, such as Anadolslyi and Saltychanslyi. These Archean-Proterozoic rocks occupy interdome synform structures [8].

Table 1. Schematic stratigraphic table representing the main rock complexes (modified from [7]).

Age	Complex/ Structure	Represented by	Thickness	Mineralization
AR	Plagiomigmatites and plagiogranite-gneiss	Shevchenkivskyi, Remivskyi granitoid complexes		
PR?	Dibrova structure	Lower tier: metapsepho-psammitic quartzites, metaconglomerates	90–320 m	U-Th-REE Dibrova mineralization
		Middle tier: ferruginous quartzites	150–210 m	
		Upper tier: gneissic rocks	150–500 m	

The Azov Megablock and consequently the Vovchansky Block are broken down by numerous faults and shear zones (Figures 1 and 2). The Dibrova mineral deposit is located at the complex tectonic junction/intersection of the Devladvivska fault zone and a series of NE- and NW-oriented faults [10].

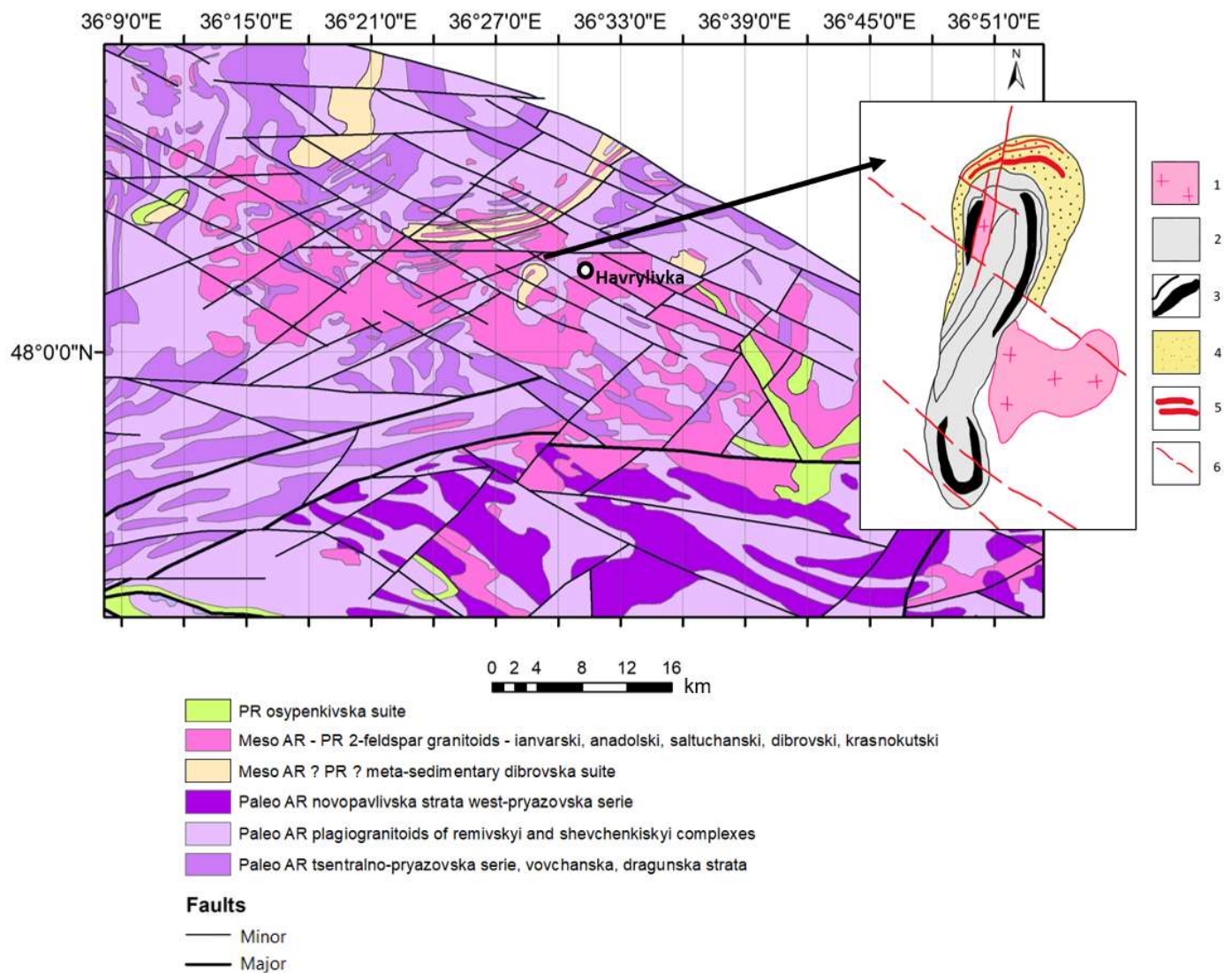


Figure 2. Geological setting of the Dibrova mineral deposit with the close-up to the schematic map of the mineral deposit (modified from [8,9]). 1—two-feldspar granitoids (biotite and muscovite-rich); 2—aluminosilicate and ferruginous schists and crystalline schists (biotite, amphibole-biotite, magnetite-cumingtonite-rich, etc.); 3—horizons of chemogenic iron-rich quartzites; 4—stratum of monoquartz and K-feldspar-bearing metasandstones, metagritstones, quartzites, with intercalations of metaconglomerates and high alumina shales; 5—stratiform U-Th-REE mineralization; 6—faults. Abbreviations: AR = Archean; PR = Proterozoic.

3. Deposit Geology

The Dibrova mineral deposit is located in the northern part of the Dibrova syncline. It is situated within a synclinal fold measuring approximately 4 by 2 km. The limbs of the fold have steep dips, and according to density modeling the closure of the fold is estimated to occur at a depth of 1100–1500 m. The fold itself consists of supracrustal rocks that have undergone metamorphism predominantly under amphibolite facies conditions, with localized occurrences of granulite to epidote-amphibolite facies [8,9]. The mineralization at Dibrova is associated with the unconformity surface between the Archean plagiogranitoid basement and the Paleoproterozoic metamorphosed sedimentary and volcanogenic-sedimentary complexes. The Dibrova mineralized zone is confined to the metasedimentary quartzites of the Dibrova suite, which with angular and stratigraphic unconformity lie on the irregular erosional surface of the Shevchenkivskiyi complex of Archean granitoids. The ore bodies consist of variably deformed (pinch and swell) vein-like bodies (Figure 3) composed of

microcline-quartz metasedimentary quartzites and pegmatoids. These veins/bodies are oriented subparallel to the strike of the host Paleoproterozoic metasedimentary rocks. REE, Th, and U are primarily found in monazite and brannerite, and to a lesser extent in minerals such as zircon and uraninite, among others. The monazite mineralization is predominantly observed in quartzites, but is also present in pegmatoid rocks.

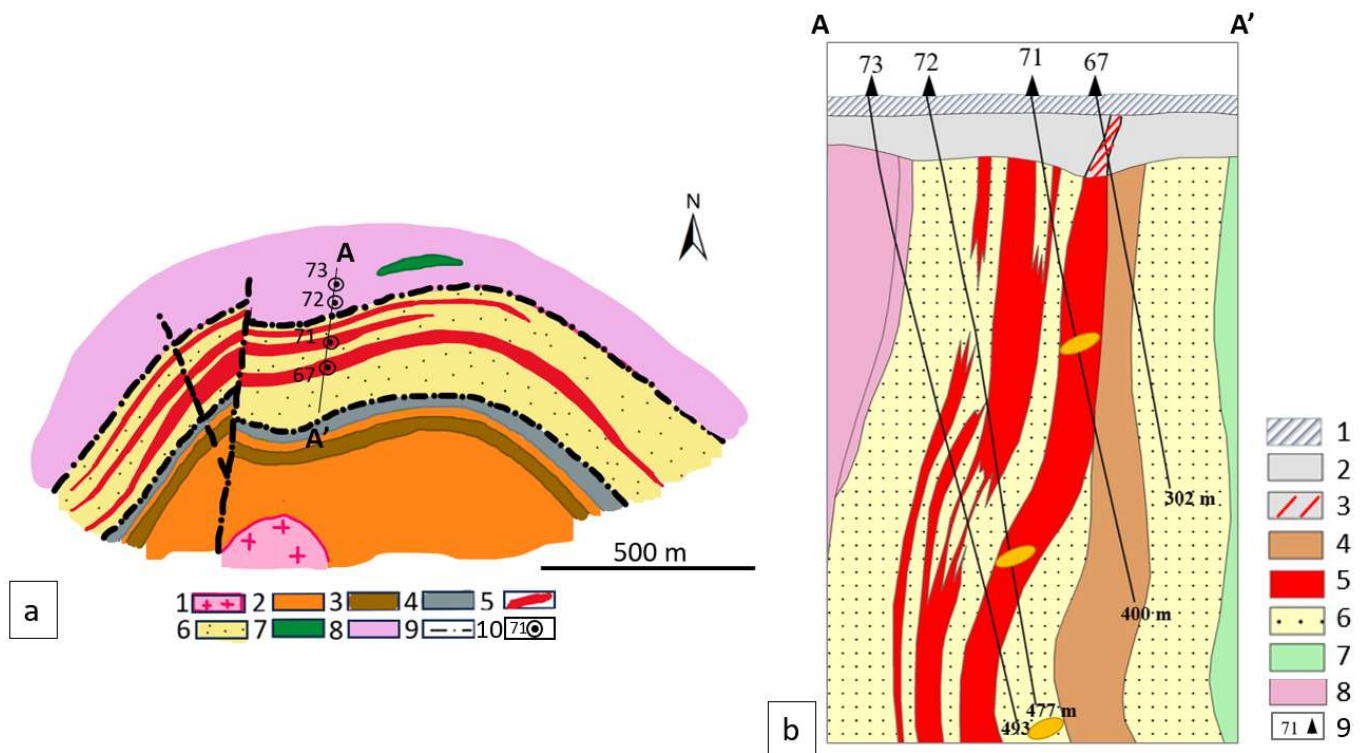


Figure 3. Dibrova mineral deposit: (a) Plan view (modified from [21]): 1—granites; 2—biotite and garnet-biotite gneisses; 3—garnet-biotite shale with magnetite; 4—garnet-amphibole-biotite shale; 5—ore zones in quartzites; 6—sillimanite-biotite, biotite, garnet-biotite, amphibole-biotite, muscovite, and fuchsite quartzites; 7—amphibolites; 8—biotite migmatite; 9—faults; 10—wells. (b) Cross-section (modified from [10]): 1—sedimentary cover; 2—weathered crust; 3—continuation of mineralization in the weathered crust; 4—garnet-quartz-amphibole-magnetite iron ore rocks; 5—mineralized zones; 6—apoconglomerate, apogritstones, apopsammite sillimanite-biotite, sillimanite-muscovite, and fuchsite quartzites with feldspars and pyrite; 7—amphibole-biotite schists; 8—biotite migmatite; 10—wells. Orange ovals mark the location of some of the studied samples.

Within quartzites, mineralization is associated with its muscovite-sillimanite-quartz varieties. Among the quartzites, some drill holes have intersected magnetite-bearing crystalline schists, as well as biotite gneisses. Biotitized, microcline-rich, and pyritized quartzites are also encountered. Small veins and lenses of biotite-microcline aplitic-pegmatitic rocks, granites, and isolated bodies of ultrabasic rocks are common [10]. Semka et al. [13] identified the following paragenetic ore mineral associations, from higher to lower temperature: assemblage 1) (zircon + monazite) ± rutile, assemblage 2) (uraninite + brannerite) ± molybdenite ± pyrite-1, assemblage 3) (pyrrhotite + bismuth + bismuthine), and assemblage 4) (pyrite-2 + galena + chalcopyrite + sphalerite). The mineralization forms three parallel ore zones both in plan and in cross-section: upper, middle, and lower zones, which extend laterally for 1700 m. The vertical extent of the preserved mineralization, unaffected by erosion, reaches 700 m. The thickness of the uranium ore zones varies: the upper zone reaches 25–30 m, the middle zone ranges from 15–20 m, and the lower zone averages around 5 m [7,16].

One of the important ore-controlling factors is the spatial position of the mineral deposit relative to the Devladiivska mantle-crustal deep sublatitude shear zone. Blastocataclastic and blastomylonitic rocks are widely developed within this zone. The mineral deposit is directly adjacent to the Dibrova secondary fault of the shear zone, a normal fault that cuts the Dibrova fold. This shear zone served as the pathway for the fluids from depth and contributed to the formation/enrichment of the mineralization. The shear zone was reactivated several times, starting from the Neoproterozoic [10]. As a result of large-scale folding during the Paleoproterozoic (ca. 2.1–2.0 Ga), the rocks that make up the fold have acquired vertical and even locally reversed dips. The northern limb of the fold (which is associated with the Dibrova fault), with its primary mineralization, has undergone a multi-stage process of dislocation metamorphism. As a result, the quartzites are characterized by the presence of conformable faults, schistose, cataclastic, mylonitized, and folded polyphase tectonites [10,17] (Figure 3).

4. Methods

Following the extensive petrographic study, four representative thin-sections were selected from a larger suite of thin sections from selected samples—72-355 (drill-hole No. 72, depth—355 m)—quartzite, 71-204 (drill-hole No. 71, depth—204 m)—quartzite, 70-258 (drill-hole No. 70, depth—258 m)—pegmatoid, 72-478 (drill-hole No. 72, depth—478 m)—biotite schist (Figure 3), with emphasis given to studying/analyzing the monazite grains. The authors referred to the guidelines provided by [22] to interpret the monazite textures and associated ages of Dibrova samples. Thus, the sizes, contours of the grains, and their internal structures in backscattered electron imaging gray tones have been assessed.

The thin sections were then analyzed using the micro-XRF-Bruker M4 Tornado μ XRF (Billerica, MA, USA). Selected monazite grains were chosen for further characterization by using a high-resolution scanning electron microscope (TESCAN VEGA3, TESCAN GROUP, Brno-Kohoutovice, Czech Republic). As a result, high-resolution images (backscattered electron (BSE)) of individual monazite grains were obtained which helped identify and characterize any zonation, heterogeneities, or inclusions in individual monazite grains. CAMECA SX100 electron microprobe (CAMECA SAS, Gennevilliers Cedex, France) was used at the SCMEM (Common Service of Electron Microscopy and X-ray Microanalysis) facilities at the GeoRessources laboratory (University of Lorraine, Nancy, France) to perform the quantitative spot analyses of monazite grains. Monazite was analyzed for a number of elements: Si, P, Ca, Y, La, Ce, Pr, Nd, Sm, Gd, Pb, Th, and U at HV (kV) = 20 and a beam current of 100 nA. A total of 151 spot analyses were recorded. Information on standards used as well as the detection limits for the analyses performed for this study is included in the Supplementary Material (Table S1).

Even though the EPMA does not measure isotopic ratios, it is possible to date the accessory minerals rich in U and Th based on elemental concentrations (e.g., monazite) [23–29]. The selected method was explained in detail by [24,30]. This method of “chemical dating” uses the measurement of Pb, Th, and U mass concentrations to allow an age to be calculated from each spot analysis. Monazite is one of the most common minerals that is dated using the EPMA-based “chemical dating” technique [31]. Thus, the monazite dating was carried out on selected monazite grains, as presented in the Results section and in the Supplementary Data (Table S1).

5. Results

5.1. Petrography

In this study, we focused our attention on characterizing and analyzing the monazite-bearing rocks—quartzites, pegmatoids, and biotite gneiss. The latter comprises the samples from outside of the main mineralization zone.

Quartzites—the main mineralization hosting rock type. They are medium- to coarse-grained (with relics of primary clastic grains; quartz fragments up to 8 cm were found [7])

grey rocks, and are often characterized by banded structure (in macro samples the average thickness of bands equals 2–5 mm) (Figures 4–6).

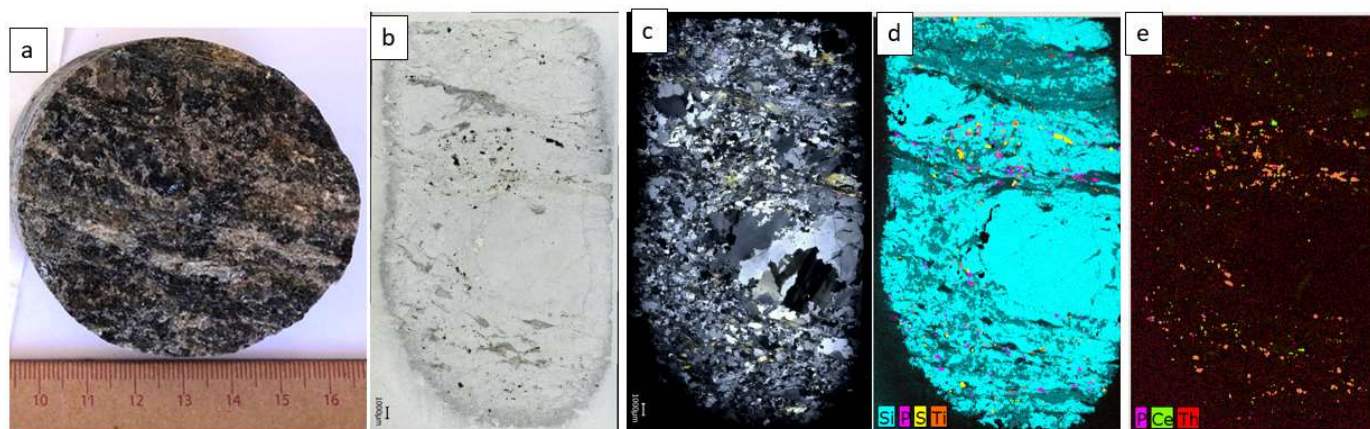


Figure 4. Sample 71-187 (drill-hole No. 71, depth—187 m)—quartzite: (a) sample photograph; (b) thin section—transmitted plane polarized light photomicrograph (PPL); (c) transmitted cross polarized light photomicrograph (XPL); (d) Micro-XRF image—Si, P, S, Ti; (e) Micro-XRF image—P, Ce, Th—can serve as an equivalent to monazite. Mineral composition: quartz 80 vol.%; muscovite + sillimanite + feldspar 15 vol.%; ore minerals 5 vol.%. Note that the ore minerals are localized in the form of scattered grains in the grain interstices.

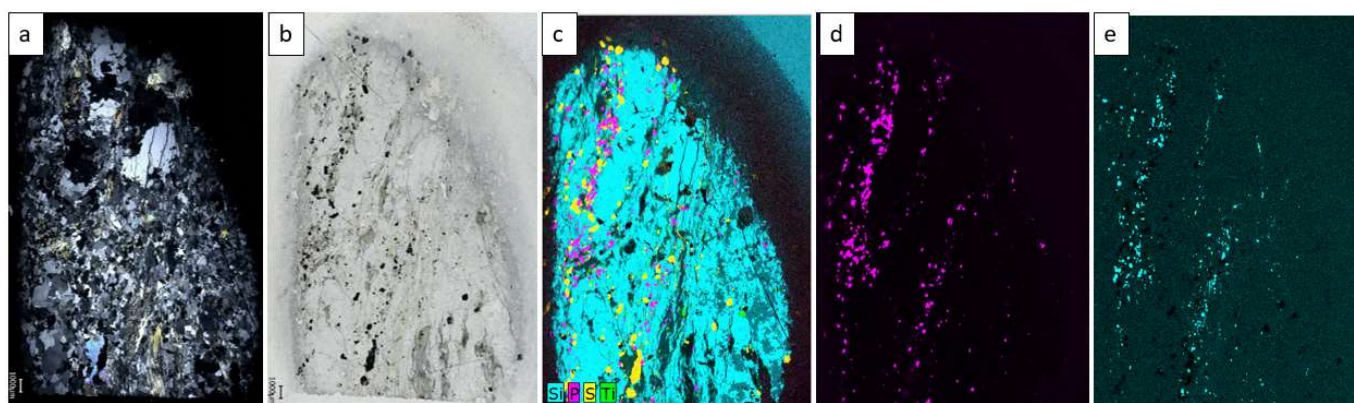


Figure 5. Sample 71-204 (drill-hole No. 71, depth—204 m)—quartzite: (a) transmitted cross polarized light photomicrograph (XPL); (b) transmitted plane polarized light photomicrograph (PPL); (c) Micro-XRF image—Si, P, S, Ti; (d) Micro-XRF image—P—can serve as an equivalent to monazite; (e) Micro-XRF image—U. Mineral composition: quartz 85 vol.%; muscovite + sillimanite + feldspar 10 vol.%; ore minerals 5 vol.%. Note that the ore minerals are localized in the form of scattered grains in the grain interstices.

The mineral composition of the quartzites is variable, thus the content of rock-forming minerals varies over wide ranges, on average: quartz 50–80 vol.%; feldspar (mostly microcline) 15–20 vol.% (sometimes up to 50–75 vol.%); sillimanite 5.0–12 vol.%; muscovite (\pm fuchsite) 5.0–7.5 vol.%; biotite 0.5–2.0 vol.%; sulfides 0.5–5.0 vol.%; monazite 1.5–5.0 vol.%; zircon, apatite, rutile—trace amounts (Figure 7). Quartz and feldspar form grains up to >5.0 mm in size. Some feldspar grains have undergone the processes of sericitization and kaolinitization. Muscovite often forms medium to coarse laths and is associated with sillimanite, monazite, and uranium minerals. Sillimanite forms fibrous crystals (fibrolite) up to >1 mm long. Mineralization is mostly found in monazite (Th-REE), and brannerite (U), but also in zircon and uraninite. Ore zones are characterized by an increase in monazite content up to 18 vol.%.

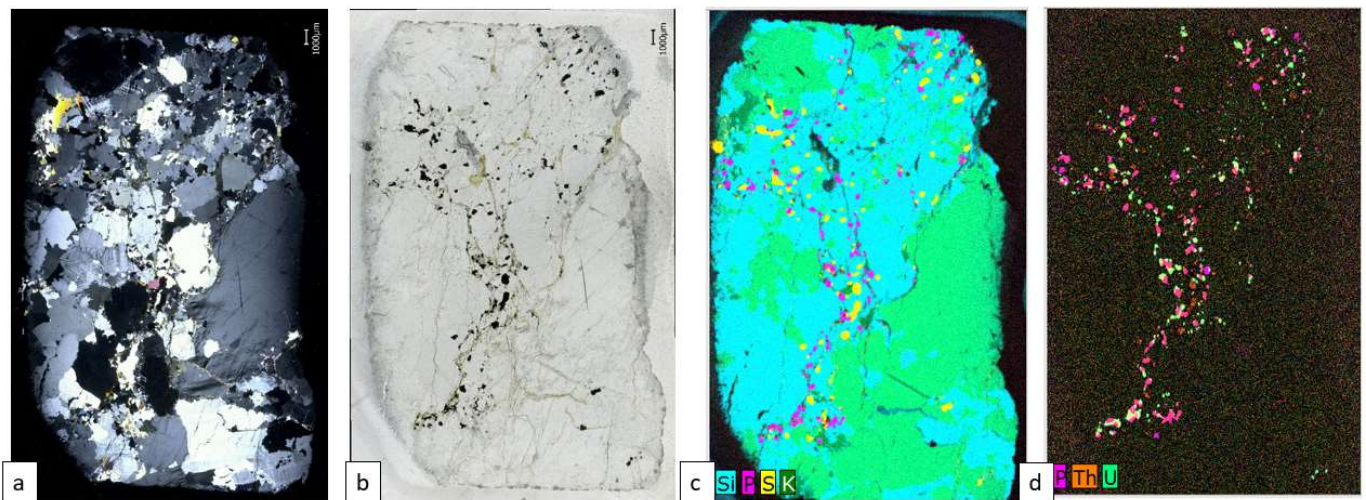


Figure 6. Sample 72-355 (drill-hole No. 72, depth—355 m)—quartzite: (a) transmitted cross polarized light photomicrograph (XPL); (b) transmitted plane polarized light photomicrograph (PPL); (c) Micro-XRF image—Si, P, S, K; (d) Micro-XRF image—P, Th, U. Note that it is clearly visible that monazite is localized in the form of scattered grains in between the quartz and microcline grains. Mineral composition: quartz 45 vol.%; muscovite + sillimanite 5 vol.%; feldspar 45 vol.%; ore minerals 5 vol.%.

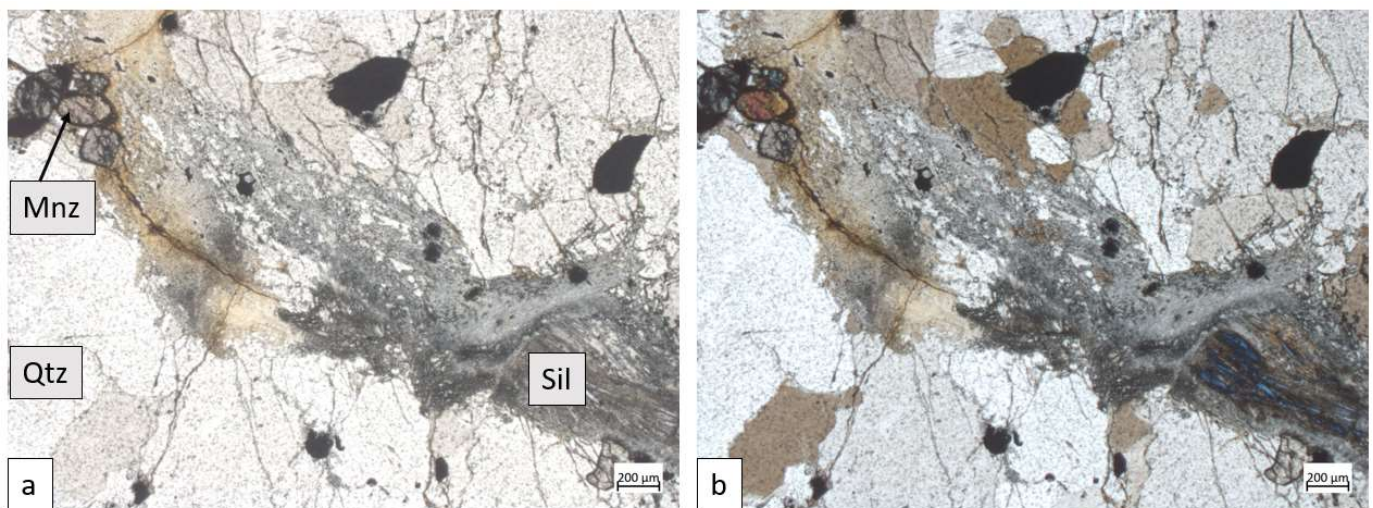


Figure 7. Sample 72-355: (a) transmitted plane polarized light photomicrograph (PPL); (b) transmitted cross polarized light photomicrograph (XPL). Abbreviations: Mnz = monazite, Sil = sillimanite, Qtz = quartz. Note that the ore minerals are associated with sillimanite and are localized in grain interstices and fracture zones.

Apart from the quartzites, the U-Th-REE mineralization is found in pegmatoids (Figures 8 and 9) within quartzites. Pegmatoids form small vein-like bodies inside quartzites, concordant with bedding. Contacts of pegmatoid bodies with the quartzites are not sharp due to intense cataclasis and dislocation metamorphism.

Pegmatoids are medium- to coarse-grained quartz-feldspar rocks and are reddish/pinkish in color. The mineral composition of the mineralized pegmatoid is quartz (15–50 vol.%), feldspar (plagioclase + microcline) (30–80 vol.%), and trace amounts of monazite, sulfide, zircon, muscovite, rutile, and uranium oxides. The distribution of ore minerals is different than in the quartzites, the modal percentage as vol.% is smaller, and their spatial distribution is more chaotic.

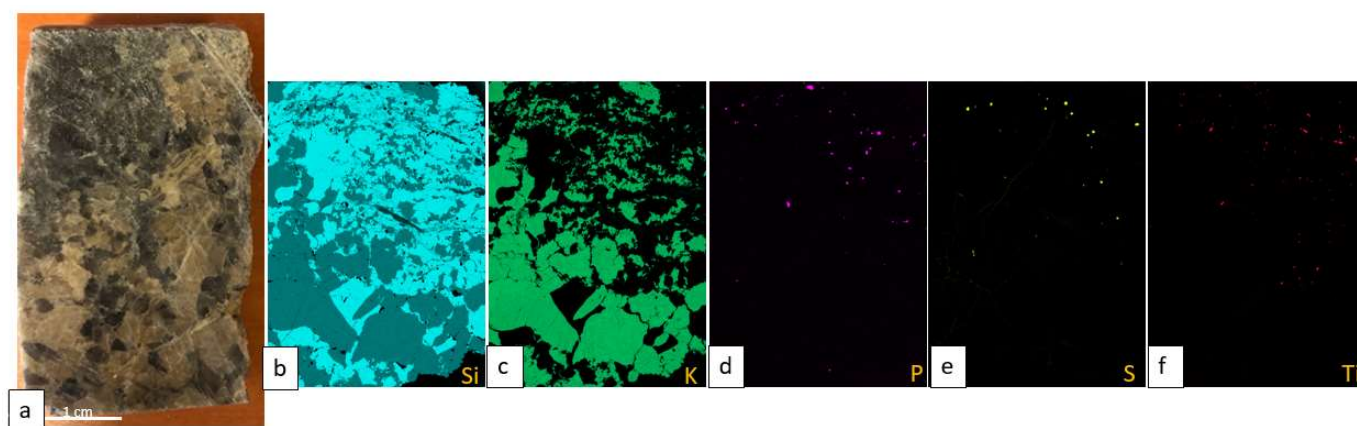


Figure 8. (a) Macro sample 70-258 (drill-hole No. 70, depth—258 m)—mineralized pegmatoid; (b) Micro-XRF image (Si) (can serve as an equivalent to quartz) of the thin-section 70-258; (c) Micro-XRF image (K)—can serve as a equivalent to feldspar; (d) Micro-XRF image (P)—can serve as an equivalent to monazite; (e) Micro-XRF image (S)—can serve as an equivalent to pyrite; (f) Micro-XRF image (Ti)—can serve as an equivalent to brannerite. Note that the distribution of ore minerals differs significantly from their distribution in quartzites. Mineral composition: quartz 50 vol.%; feldspar 48 vol.%; ore minerals ca. 2 vol.%.

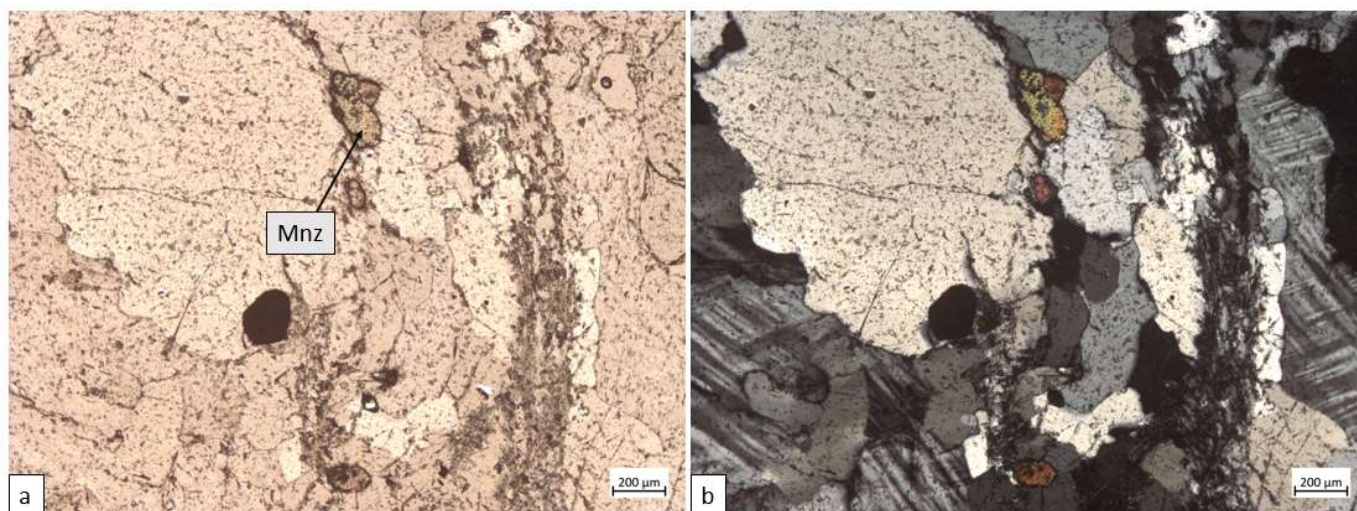


Figure 9. Monazite grains in pegmatoid. Sample 70-258 (mineralized pegmatoid): (a) transmitted plane polarized light photomicrograph (PPL); (b) transmitted cross polarized light photomicrograph (XPL). Abbreviations: Mnz = monazite.

We have also studied a biotite schist/gneiss sample (drill-hole No. 72, depth—478 m) (Figure 10). The rock is a metamorphic product of metapelitic sediments. It is composed of biotite (40 vol.%), quartz (30 vol.%), garnet (20 vol.%) (not shown on the thin-section in Figure 10b–e), sulfides (10 vol.%), and trace amounts of monazite and zircon. Monazite grains are scattered in the rock and reach 50 to 100 μm length in size.

5.2. Monazite Chemistry and Characterization

Monazite ((Ce, La, Th)PO₄) is a mineral found within ore bodies, in both pegmatoids and quartzites. The modal percentage as vol.% of this mineral can vary significantly, ranging from isolated grains to substantial concentrations, comprising up to 15–18 vol.% [13] of the overall rock volume within the ore bodies. Monazite is often found intergrown with zircon, brannerite, and rutile (Figures 11 and 12).

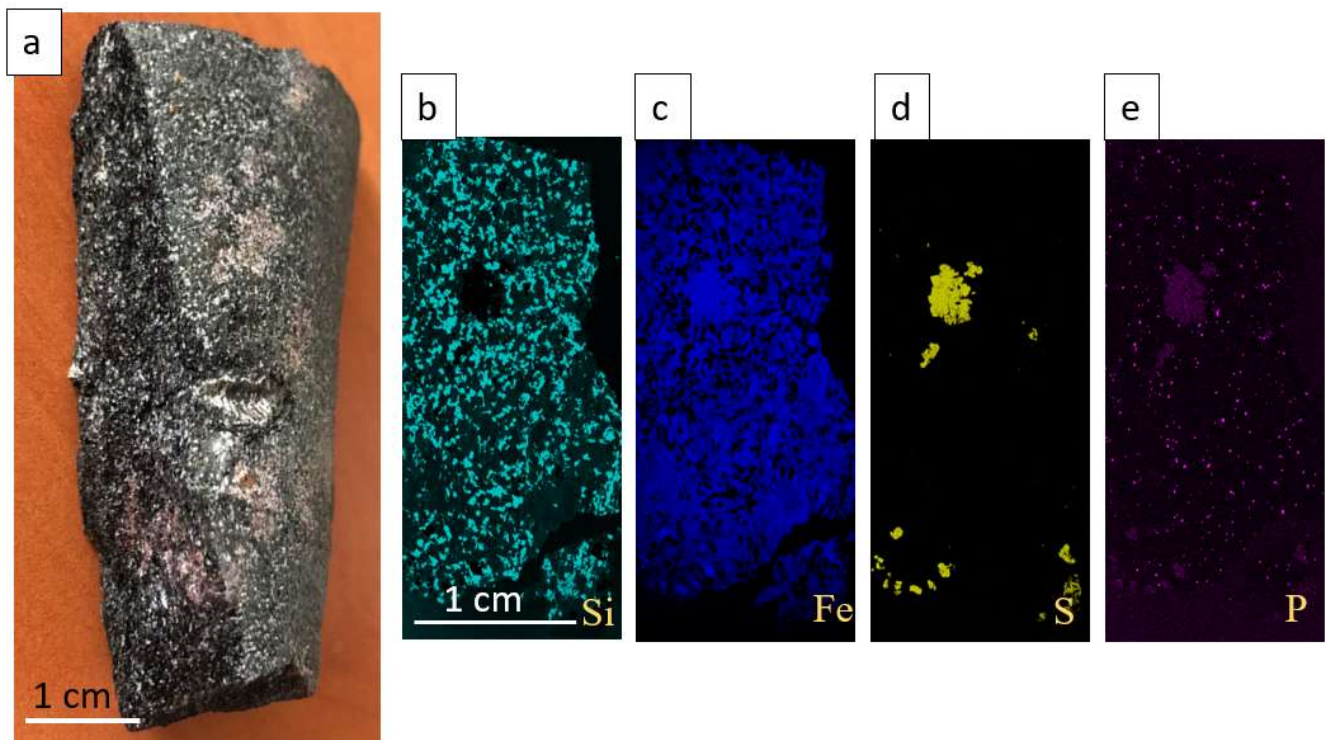


Figure 10. Garnet-biotite gneiss: (a) Sample 72-478 (drill-hole No. 72, depth—478 m)—biotite schist/gneiss; (b) Micro-XRF image (Si) (can serve as an equivalent to quartz) of the thin-section 72-478; (c) Micro-XRF image (Fe)—can serve as an equivalent to biotite; (d) Micro-XRF image (S)—can serve as an equivalent to sulfides; (e) Micro-XRF image (P)—can serve as an equivalent to monazite.

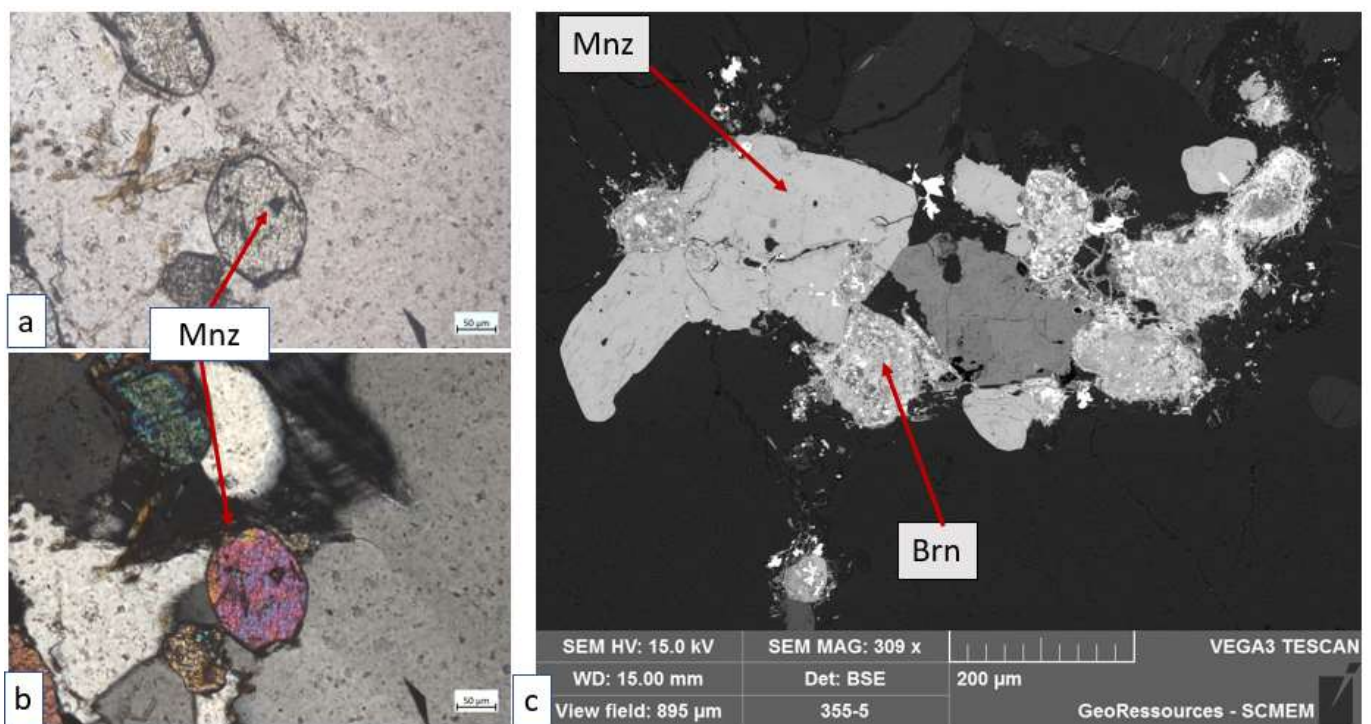


Figure 11. (a) Photomicrograph of mineralization in transmitted plane polarized light (PPL); (b) transmitted cross polarized light photomicrograph (XPL); (c) SEM-BSE image (sample 72-355). Abbreviations: Mnz = monazite, Brn = brannerite.

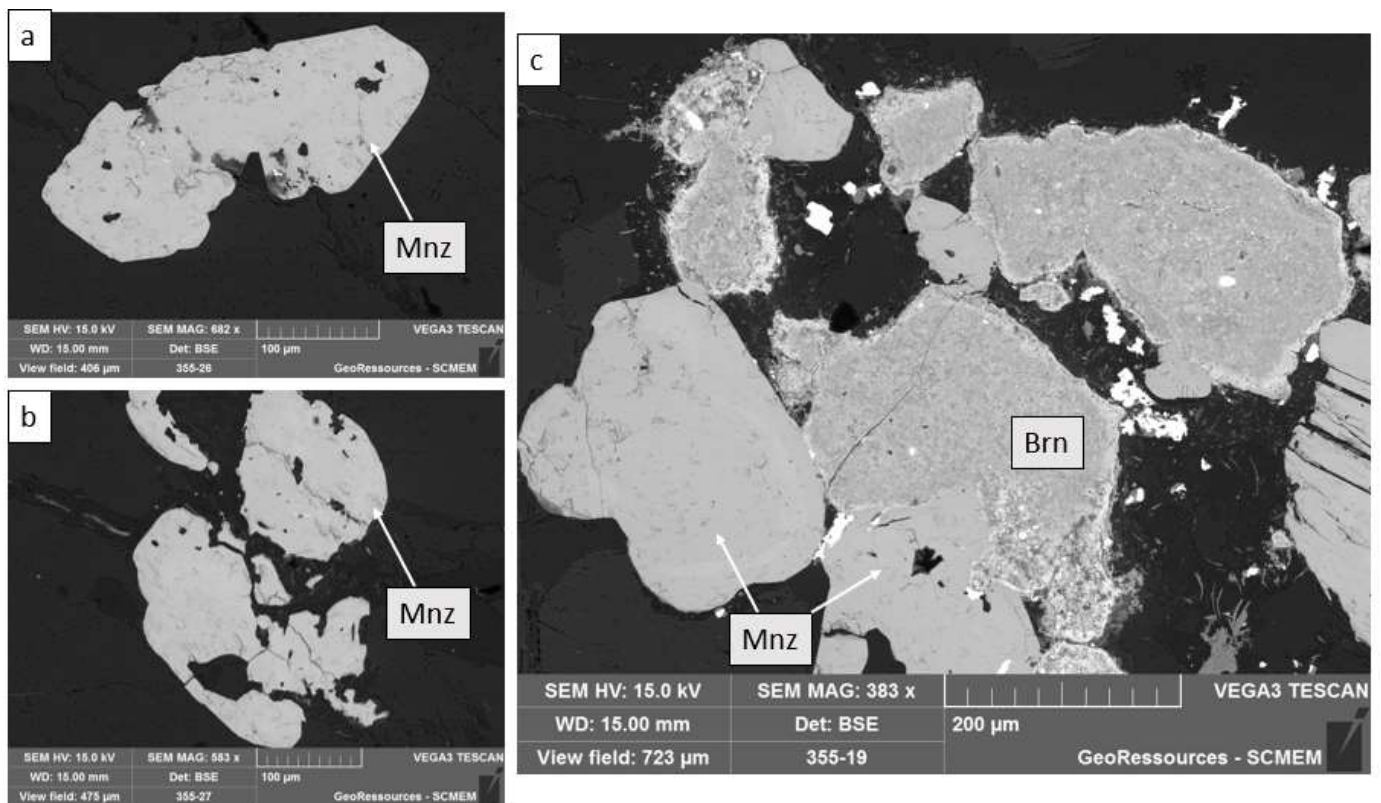


Figure 12. Clusters of monazite and brannerite grains in quartz matrix: (a–c) SEM-BSE images of monazite (sample 72-355). Abbreviations: Mnz = monazite, Brn = brannerite. Note the monazite zonation on (c), chemical dating shows that the core yields the age of 2.7 Ga, while lighter grey zone gives 2.1 Ga and rim yields 2.0 Ga.

The mineral often, but not always, occurs in grain interstices and fracture zones as branching chains and elongated clusters transitioning into veins. The individual grains exhibit diverse shapes, ranging from angular-rounded to oval forms, and can form complex elongated allotriomorphic aggregates. Grains are often corroded (Figures 11 and 12). Size of grains in the studied mineralized samples ranged up to 1 mm. Inclusions in monazite are represented by quartz and zircon.

Monazites within the pegmatoid sample are unzoned, whereas in the quartzites they exhibit ill-developed or no zonation (Figure 12c). Lighter grey zones are characterized by higher Th and U contents and lower REE contents. The chemical composition of monazite is presented in the Supplementary Data (Table S1). A total of 151 spots have been analyzed: 107 spots in the monazite from quartzite samples (sample 355: 71 spots, sample 204: 36 spots), 35 spots in the monazite of pegmatoid sample (sample 258), and nine spots from the biotite schist/gneiss sample (sample 478). Sukach et al. and Kramar et al. [8,10] stated that monazite is a cheralite type; however, the chemical EPMA analyses that we have conducted reveal that for all the studied samples, regardless of the host rock type, the monazite grains are dominated by monazite-(Ce) compositions (Figure 13a,b).

All the analyzed samples exhibit a predominance of the LREE, with Ce being the dominant REE element (Figure 13). The oxide contents (in wt.%) are presented in Table 2 and Figure 14.

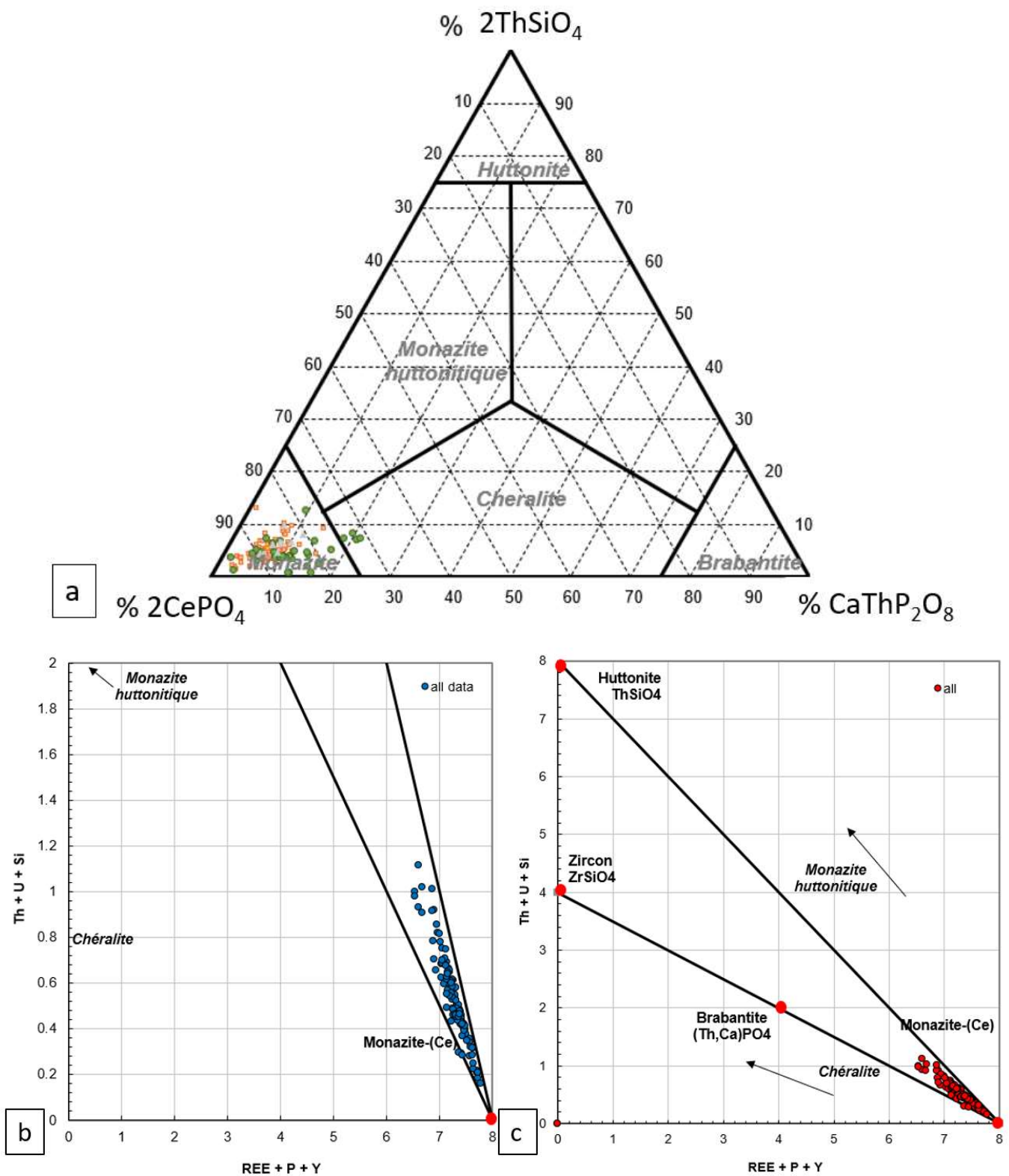


Figure 13. (a) Ternary plot of the monazite compositions (orange—quartzites, green—pegmatoid, grey—biotite schists); (b) Th + U + Si vs REE + Y + P diagram (all samples are displayed in blue (b) and red (c)). For the studied samples, the monazite grains are dominated by monazite-(Ce) compositions.

Table 2. The main oxide contents (in wt.%) by individual monazite sample. *N*—number of points analyzed.

Oxide, wt.%	Min	Max	Average 355 (Quartzite) <i>N</i> = 71	Average 204 (Quartzite) <i>N</i> = 36	Average 258 (Pegmatoid) <i>N</i> = 35	Average 478 (Biotite Schist) <i>N</i> = 9
SiO ₂	0.20	3.28	1.28	1.21	1.14	1.59
P ₂ O ₅	24.64	31.16	28.46	28.48	28.22	28.00
CaO	0.39	2.82	0.92	0.97	1.46	0.94
Y ₂ O ₃	0.00	2.74	2.27	1.41	1.65	1.56
La ₂ O ₃	11.83	19.05	14.99	16.22	15.49	14.35
Ce ₂ O ₃	14.31	33.10	28.67	28.67	26.88	27.20
Pr ₂ O ₃	2.15	3.85	2.93	2.91	2.69	2.89
Nd ₂ O ₃	6.33	12.77	9.19	8.97	8.04	9.49
Sm ₂ O ₃	0.71	2.46	1.34	1.22	1.14	1.42
Gd ₂ O ₃	0.06	1.59	1.00	0.85	0.80	0.87
PbO	0.20	1.76	0.88	0.90	0.97	0.85
ThO ₂	2.86	18.20	8.53	7.91	9.85	8.88
UO ₂	0.00	0.69	0.30	0.17	0.20	0.37

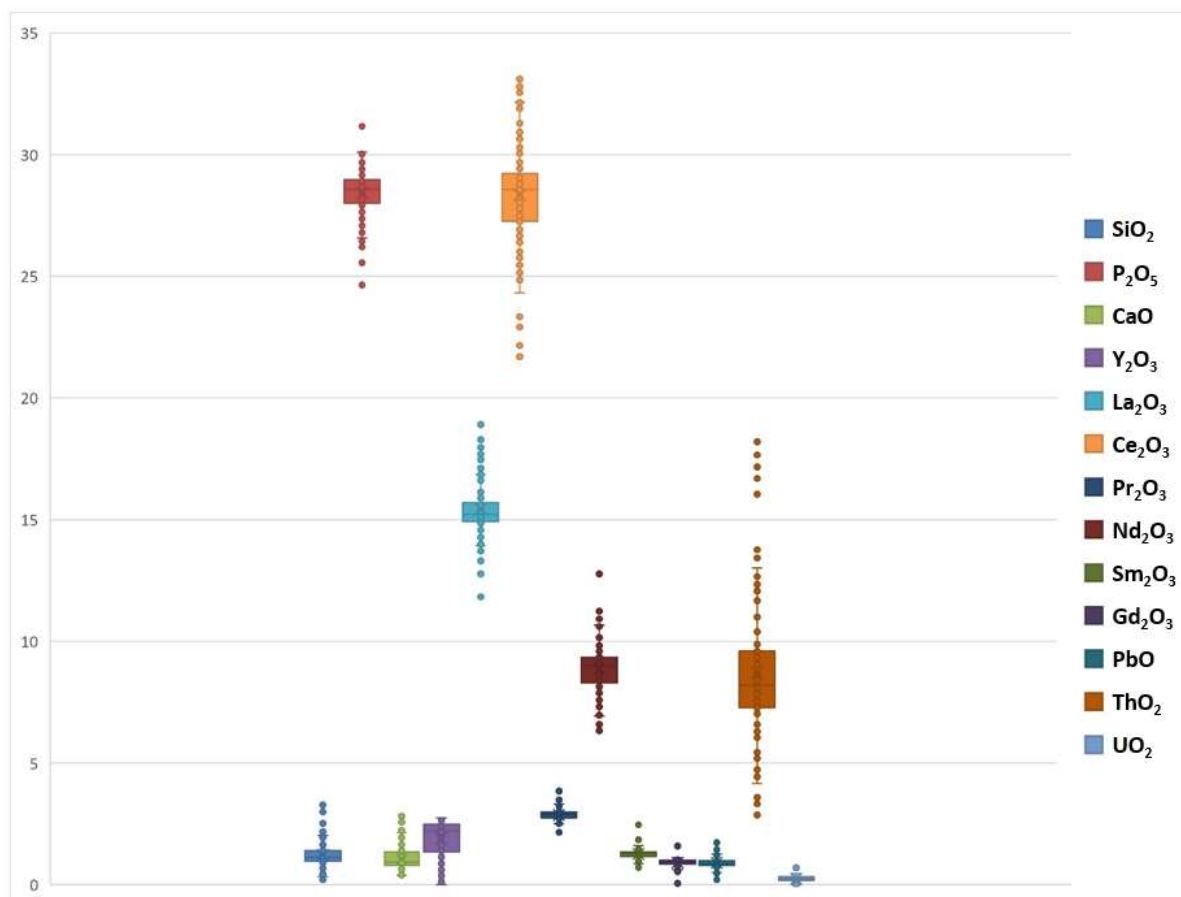


Figure 14. Box and whisker plots of main oxide concentrations (in wt.%) in monazites. Different colors represent different oxides (see legend to the left of the graph). Number of spots analyzed = 142, representing quartzite and pegmatoid samples.

Correlation analysis was conducted to detect any direct or inverse correlations for all the studied monazite grains, as well as for the specific host rocks. Strong direct correlation is observed for ThO_2 and PbO , SiO_2 ; Nd_2O_3 and Ce_2O_3 , Pr_2O_3 , Sm_2O_3 . Strong inverse correlation is observed for P_2O_5 and SiO_2 ; Ce_2O_3 (similar for other REE) and CaO , PbO , ThO_2 . UO_2 exhibits weak direct correlation with Y_2O_3 and shows no correlation (to very weak inverse) to REE (Figure 15).

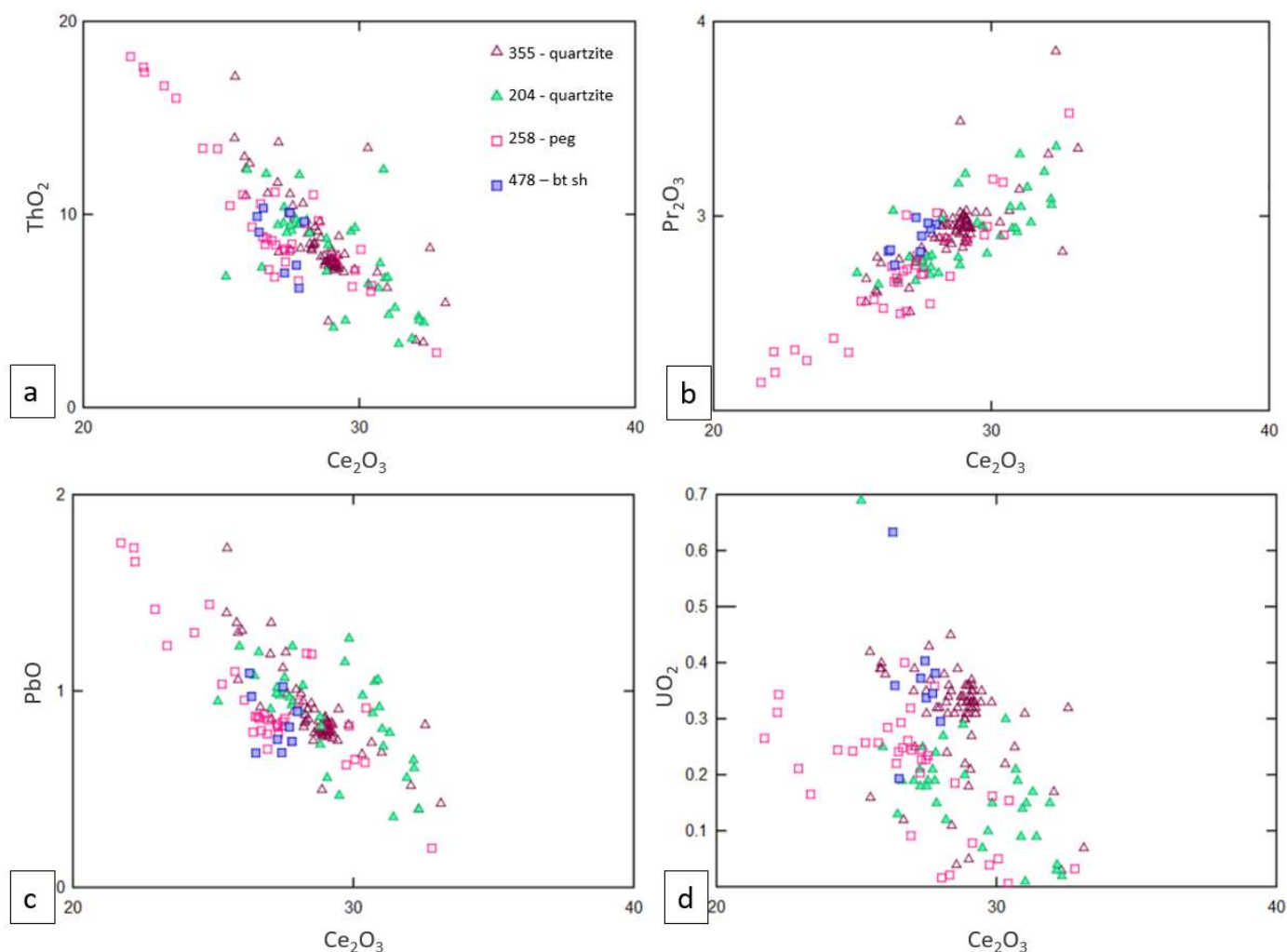


Figure 15. (a) ThO_2 to Ce_2O_3 (in wt.%) graph—inverse correlation observed for all lithologies; (b) Pr_2O_3 to Ce_2O_3 (in wt.%) graph—direct correlation observed for all lithologies; (c) PbO to Ce_2O_3 (in wt.%) graph—inverse correlation observed for all lithologies; (d) UO_2 to Ce_2O_3 (in wt.%) graph—no correlation to very weak inverse (355—quartzite sample, 204—quartzite sample, 258—pegmatoid sample, 478—biotite schist sample).

We have analyzed the monazite grains in each sample individually (Figures 16–19: a—main oxide content distributions in wt.%, b—monazite main oxide concentrations (in wt.%) shown for each point analysis). Overall, we can see that there are no large differences between the oxide concentration patterns of the studied samples. However, we do see a spread in the concentration within each individual sample for such oxides as ThO_2 , Ce_2O_3 , and Nd_2O_3 .

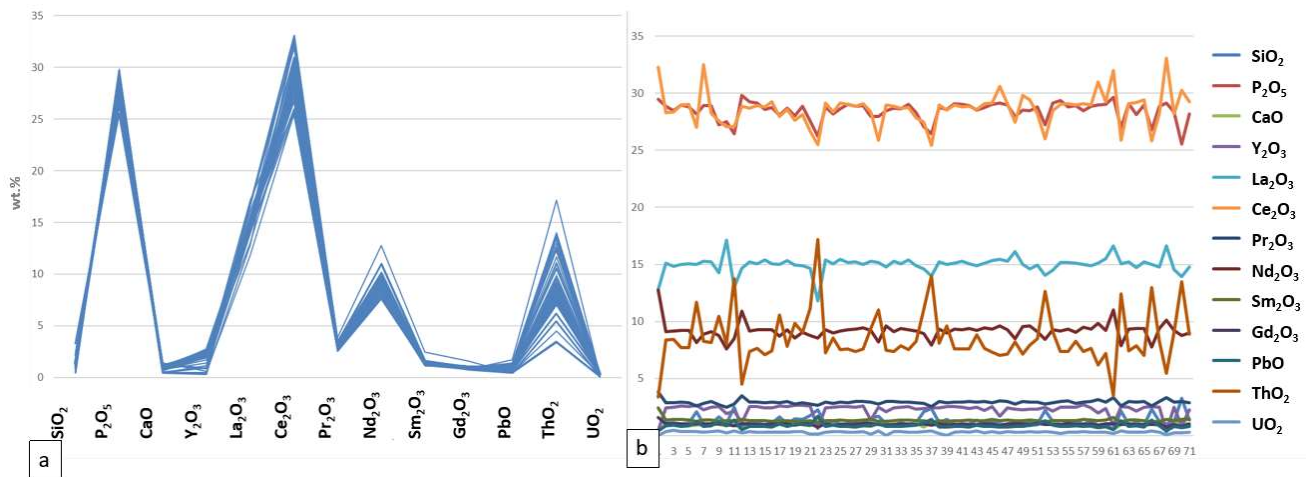


Figure 16. Sample 72-355—monazites in quartzite: (a) Graph showing the monazite main oxide concentrations (in wt.%); (b) monazite major oxide concentrations (in wt.%) shown for each point analysis. Different colors represent different oxides.

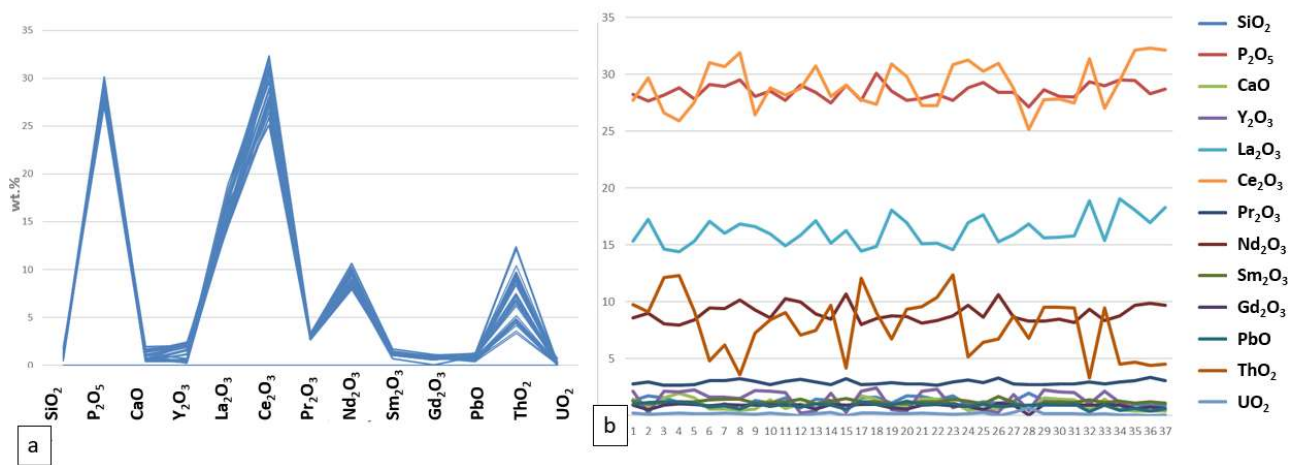


Figure 17. Sample 71-204—monazites in quartzite: (a) Graph showing the monazite main oxide concentrations (in wt.%); (b) monazite major oxide concentrations (in wt.%) shown for each point analysis. Different colors represent different oxides.

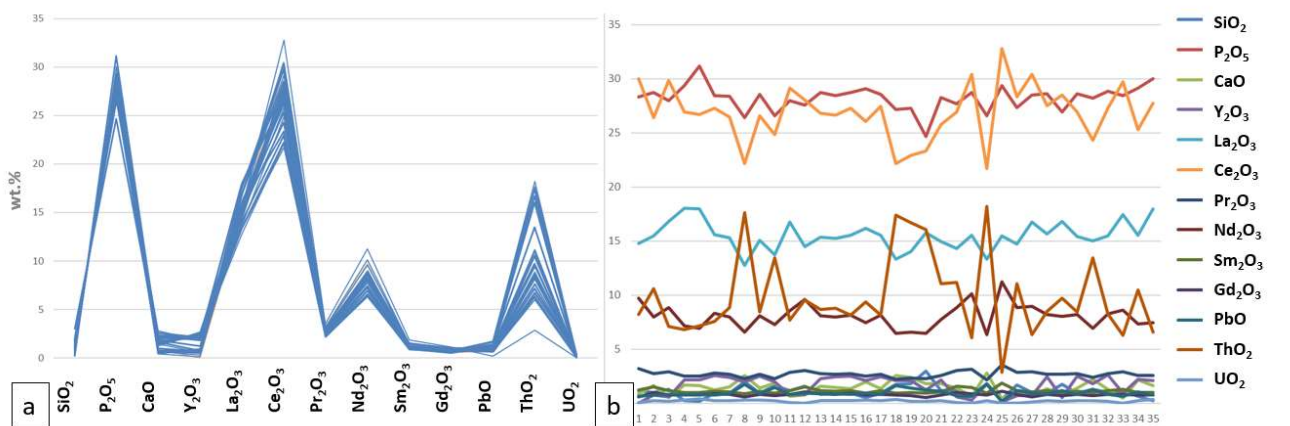


Figure 18. Sample 70-258—monazites in pegmatoid: (a) Graph showing the monazite main oxide concentrations (in wt.%); (b) monazite major oxide concentrations (in wt.%) shown for each point analysis. Different colors represent different oxides.

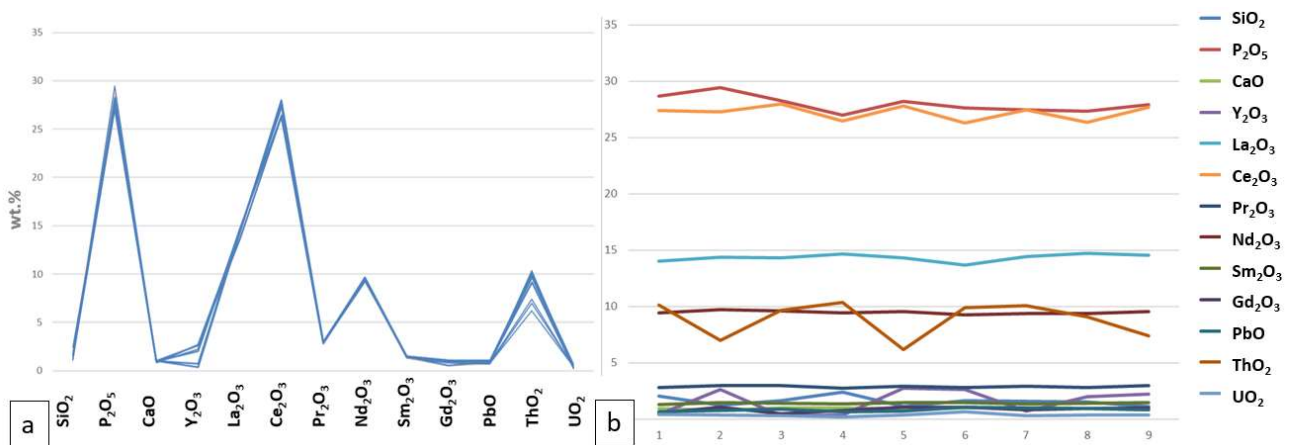


Figure 19. Sample 72-478—monazites in biotite schist: (a) Graph showing the monazite main oxide concentrations (in wt.%); (b) monazite major oxide concentrations (in wt.%) shown for each point analysis. Different colors represent different oxides.

5.3. U-Th-Pb Chemical Dating

In this research, the chemical ages were calculated using the EPMA data and the procedures of [24,30,32]. Data are provided in the Supplementary Data (Table S1). The graphs in Figure 20 and Table 3 show the obtained chemical U-Th-Pb ages for monazites from all the studied rock types—quartzites, pegmatoid, and biotite schist. These ages can be interpreted as the age of the peak metamorphism/metasomatism, magmatic crystallization, and/or possible age of the source rock area. The majority of chemical ages (U-Th-Pb) calculated from monazite EMPA range between 2.2–2.0 Ga.

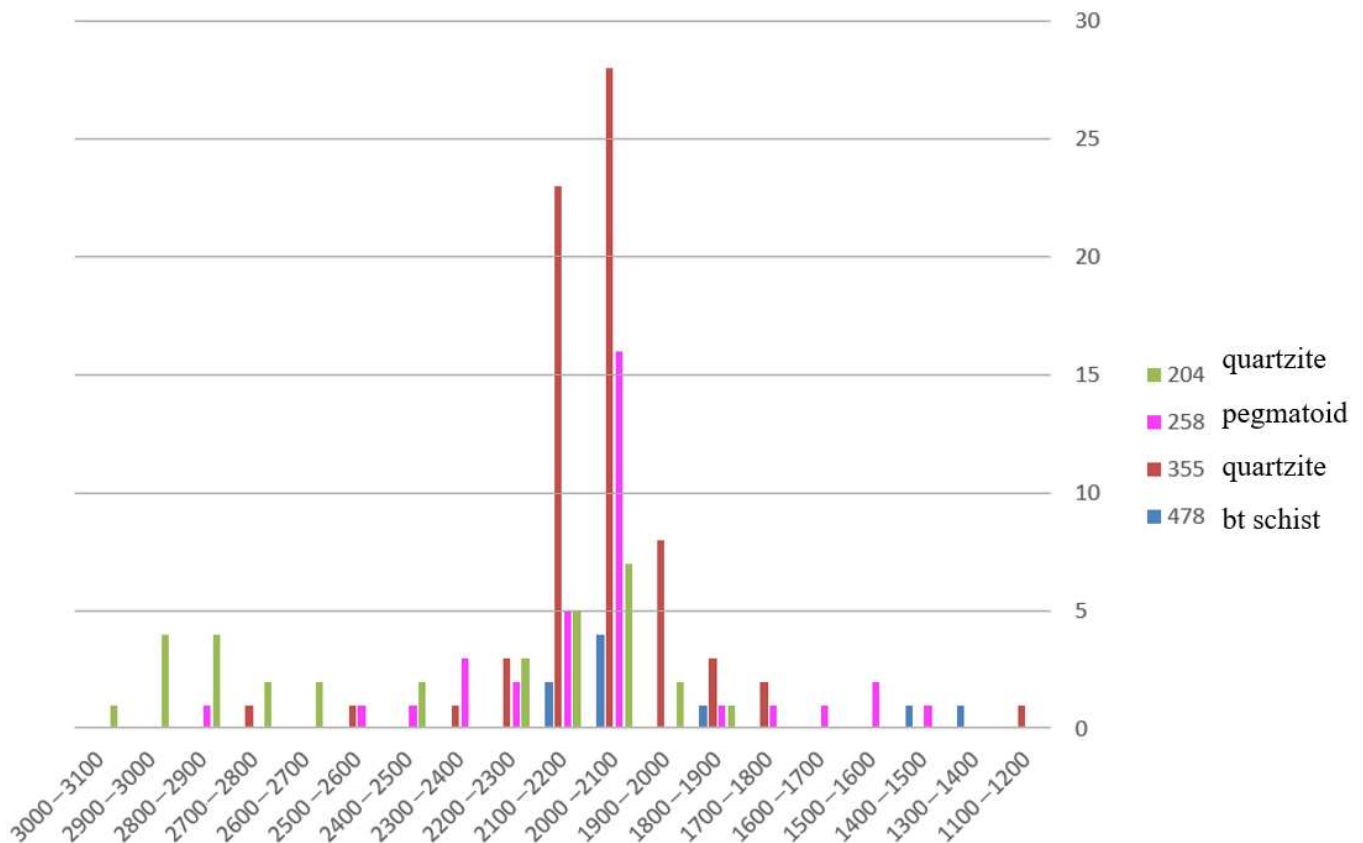


Figure 20. Density distribution of monazite chemical dating results. Main age groups identified: 3.0–2.8 Ga and 2.3–1.9 Ga.

Table 3. Count to chemical age by 100 Ma intervals.

Age Range, Ma	Quartzite 204, Count	Pegmatoid 258, Count	Quartzite 355, Count	Biotite Schist 478, Count	Grand Total
1100–1200			1		1
1200–1300					0
1300–1400				1	1
1400–1500		1		1	2
1500–1600		2			2
1600–1700		1			1
1700–1800		1	2		3
1800–1900	1	1	3	1	6
1900–2000	2		8		10
2000–2100	7	16	28	4	55
2100–2200	5	5	23	2	35
2200–2300	3	2	3		8
2300–2400		3	1		4
2400–2500	2	1			3
2500–2600		1	1		2
2600–2700	2				2
2700–2800	2		1		3
2800–2900	4	1			5
2900–3000	4				4
3000–3100	1				1
Total	33	35	71	9	148

We can also observe different age trends for different rock types—the biggest peaks for quartzites yield age ranges of 2.2–2.0 Ga and 3.0–2.8 Ga; for monazites in pegmatoid sample—2.1–2.0 Ga, and for monazites in biotite schist/gneiss—2.1–2.0 Ga.

Ce₂O₃, UO₂, and ThO₂ to chemical age graphs were created to observe any changes in their concentrations through time (Figure 21). It was noted that around 2.0 Ga the Ce concentrations have decreased overall for the studied samples, whereas the U and Th concentrations have increased.

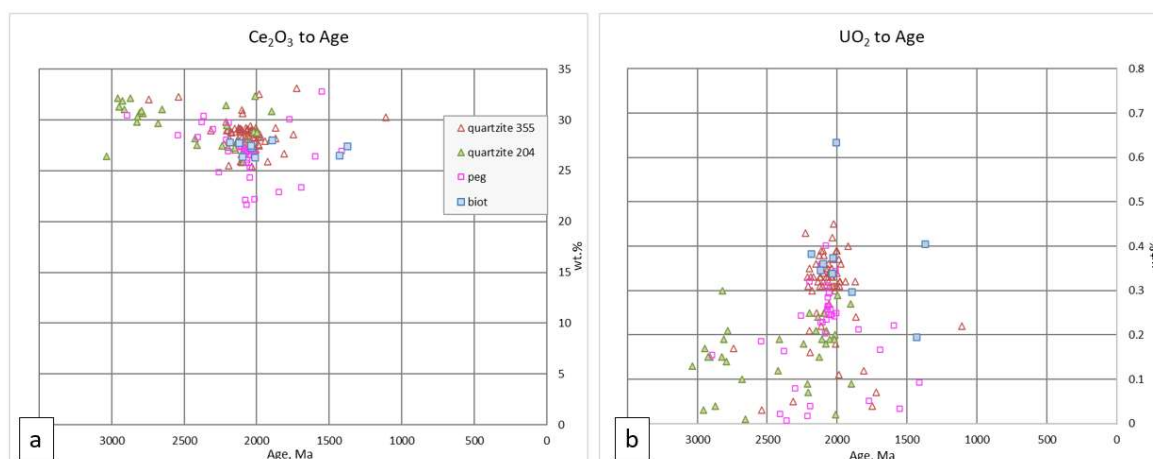


Figure 21. Cont.

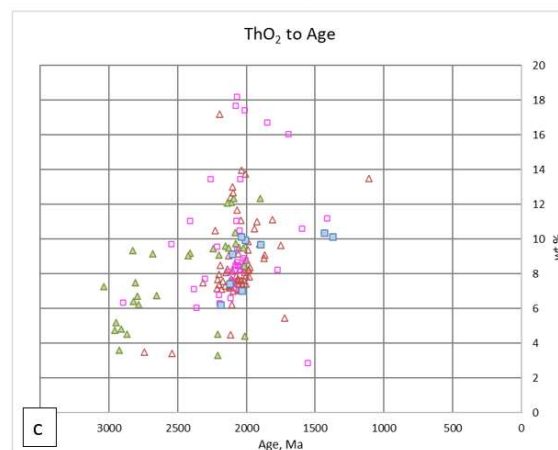


Figure 21. Monazite oxide concentration graphs: (a) Ce_2O_3 to chemical age by lithology; (b) UO_2 to chemical age by lithology; (c) ThO_2 to chemical age by lithology. We can observe the increase in U and Th concentrations in monazites from all lithological units and a relative decrease in REE.

6. Discussion

6.1. The Complex Genesis of the Dibrova Mineralized Area and Hypotheses Regarding the Formation of Primary Mineralization

It is suggested that the primary mineralization within the quartzites (which at the time of formation could have comprised clastic rocks—gravels and sandstones with rare pebbles) was formed as a result of denudation and transfer of Archean granitoids of the Shevchenkivskiy complex. Later, these sedimentary rocks underwent amphibolite facies metamorphism and transformed into ore-bearing quartzites [10]. Evidence for syn-metasedimentary genesis of primary mineralization can be seen from the presence of relic sandstone-gravel-like structures in quartzites, which are shown in some of the representative figures from this study (Figures 4–6 comparable to findings documented by [7,9]). In addition, the mineral deposit is characterized by sedimentary layered morphology of ore bodies (in the form of stratified horizons—Figure 3), and monazite (enriched in REE, Th, and U) is considered the main ore mineral during the formation of primary mineralization, as well as zircon—typical placer minerals.

The whole-rock geochemistry data show different geochemical trends for quartzites and pegmatoids and the absence of transitional varieties (for example, Figure A1a in Appendix A, which shows the correlation between the content of titanium oxide and silicon oxide). Such a difference allows us to conclude that these two rock types most likely have different origins and that quartzites may have a primary sedimentary genesis.

However, it is worth mentioning that the main stage of development of the mineralization of the mineral deposit is related to secondary tectono-magmatic reactivation processes during the Paleoproterozoic, including high-temperature metasomatism, which most researchers agree on, regardless of the proposed hypothesis of the origin of the primary mineralization.

6.2. The Role of the Devladiivska Deep Mantle-Crustal Fault Zone and Paleoproterozoic Tectonomagmatic Activation in the Formation of Mineralization

One of the important ore-controlling factors is the spatial position of the mineral deposit in relation to the Devladiivska mantle-crustal deep sublatitude shear zone. The relationship between uranium mineralization of different genesis and deep regional fault zones is also observed in other uranium provinces in the world, e.g., the Athabasca one within the Canadian Shield [33]. Paleoproterozoic tectono-magmatic activation (2.0–2.1 billion years ago) is characterized by an increased background uranium content in the rocks of the Azov Megablock and formation of most of the Na-metasomatic uranium deposits [34].

Within the Devladvivska deep mantle-crustal fault zone, the primary mineralized ore bodies were transformed without significant change in their sedimentary-layered morphology. The remobilization and enrichment of mineralization is associated with various stages of reactivation of the Devladvivska deep fault zone that stretched over time from the Neoproterozoic and are recorded by complex polychronous tectonites and multi-stage main and associated mineralization [10].

The remobilization of REE, uranium, and thorium is also associated with the development of potassium metasomatism during the final stages of formation of sub-alkaline granitoids of the Dibrova type. As a result of the isochemical metamorphism of the amphibolite facies, the primarily meta-sedimentary clastic kaolinite-bearing rocks were transformed into quartzites rich in sillimanite, muscovite, and fuchsite. Potassium metasomatism occurred locally, which led to microclinization resulting in the formation of large-grained aggregates of microcline. With these processes in the Proterozoic around 2.0 Ga, we observe an increase in the content of thorium and uranium (Figure 21b,c).

6.3. Dating of Monazite Grains to Decipher the History of Mineralization Formation

The dating of monazite and its separate zones allows obtaining information about the thermal and tectonic history of the study area, which in turn makes it possible to reconstruct the geological evolution of the region and establish the sequence of and connection between geological events.

Based on the petrographic studies that we have conducted, mineralization in monazites and zircons is interpreted by the authors as the oldest. Zoned monazite grains with inherited Archean cores were also recorded and dated. Uranium concentration within monazite grains rapidly increases in the Paleoproterozoic, which may indicate a redistribution and/or introduction of uranium into the mineral system.

U-Pb-Th electron microprobe chemical dating of monazites carried out in this study yielded two main age groups at 3.0–2.8 Ga and 2.2–2.0 Ga. The first group at 3.0–2.8 Ga (mainly associated with quartzite samples) may represent the time of formation of the Archean granitoids, which served as a source of monazite for its clastic sedimentation in the Dibrova suite sediments during the Paleoproterozoic. Monazite-bearing granitoid massifs of the Meso-Neoproterozoic age are widely represented in the West Azov area (for example, granites of the Shevchenkiv or Janvarskyi complexes) [9].

The next age group, 2.2–2.0 Ga, which is associated with all the studied samples, represents remobilization and subsequent enrichment of mineralization. Uranium mineralization is most likely connected with this event (according to [13], the age of uranium mineralization is 1.98 Ga). Our study documents an increase in uranium concentration in monazite around 2.0 billion years ago, supporting this suggestion. This date also reflects the time of powerful tectonomagmatic activation of the region.

Later events show further reactivations of the system, but without significant remobilization of mineralization.

In summary, the data suggest that the history of the development and remobilization at the Dibrova mineral deposit was complex and polyphase. Without discarding other hypotheses, we believe that the mineralization was probably formed by the ultrametamorphic processes that accompanied the intrusion of aplite pegmatoid granite bodies into the meta-sedimentary clastic rocks and then promoted remobilization, redistribution, and enrichment of the primary mineralization.

7. Conclusions

After conducting this mineralogical and petrographic investigation of the monazite-bearing samples from the Dibrova area, we were able to draw certain conclusions regarding the genesis and age(s) of mineralization:

- (1) Two main age groups were identified for the monazite: 3.0–2.8 Ga and 2.2–2.0 Ga. An age of 3.0–2.8 Ga is proposed as the time of formation of Archean granites with the formation of primary U-Th-REE mineralization (related to erosion of granites and sediment accumulation); an age of 2.2–2.0 Ga is proposed for the remobilization and subsequent enrichment of U-Th-REE mineralization (related to tectono-magmatic activation during the Paleoproterozoic).
- (2) Ancient monazite cores can provide evidence of Archean granites as a source of ore components during the formation of primary mineralization.
- (3) The metasepho-psammitic structures of quartzites that we discovered may indicate their primary meta-sedimentary genesis.
- (4) Whole-rock geochemistry revealed two main trends in the distribution of major oxides within pegmatoid and quartzite samples, which clearly indicates a different genesis for quartzites (meta-sedimentary) and pegmatoids (magmatic/metamorphic).
- (5) Further research is recommended to provide a better understanding of the processes that led to the formation of the Dibrova complex mineral deposit and related analogous ones.

Supplementary Materials: The following supporting information can be downloaded at: <https://www.mdpi.com/article/10.3390/min13101241/s1>, Table S1: Oxide, element concentrations, ages of monazites.

Author Contributions: Conceptualization, K.P., V.P., I.R.A., and O.I.; methodology, K.P.; validation, K.P., V.P., I.R.A., and O.I.; investigation, K.P.; resources, K.P. and V.P.; data curation, K.P.; formal analysis, K.P.; writing—original draft preparation, K.P. and V.P.; writing—review and editing, K.P., V.P., I.R.A., and O.I.; visualization, K.P.; supervision, V.P., I.R.A., and O.I.; project administration, K.P. All authors have read and agreed to the published version of the manuscript.

Funding: The analytical research in GeoRessources was supported/funded by GeoRessources research center (University of Lorraine and CNRS) and the French national PAUSE program (France, <https://www.campusfrance.org/fr/pause-programme-aide-accueil-urgence-scientifiques-exil>, accessed on 1 August 2023).

Data Availability Statement: The data presented in this study are openly available online at Supplementary Materials.

Acknowledgments: This work was carried out thanks to the equipment of the SCMEM (Common Service of Electron Microscopy and X-ray Microanalysis) of the University of Lorraine. The authors thank the GeoRessources laboratory at the University of Lorraine for access to facilities, guidance, and support. The authors are extremely grateful to the anonymous reviewers and guest academic editor for taking the time and effort to review the manuscript. All your edits and comments were incredibly helpful to improving the quality of our manuscript.

Conflicts of Interest: The authors declare no conflict of interest.

Appendix A

Appendix A.1. Whole-Rock Geochemistry

Using the data presented by [13] on whole-rock geochemistry of the main rock types of the Dibrova mineralized area, some statistical work was carried out to facilitate creation of several discrimination diagrams to explain their petrogenetic origin and to better characterize in particular the mineralized quartzites and pegmatoids. Some of the resulting discrimination diagrams are shown in Figure A1a—the SiO₂ to TiO₂ discrimination diagram. It shows two distinct different trends for the two rock types and no transitional varieties, thus suggesting different origins for the quartzite and pegmatoid samples. The same interpretation comes from factor analysis (Figure A1b,c), whereby two distinct trends are observed.

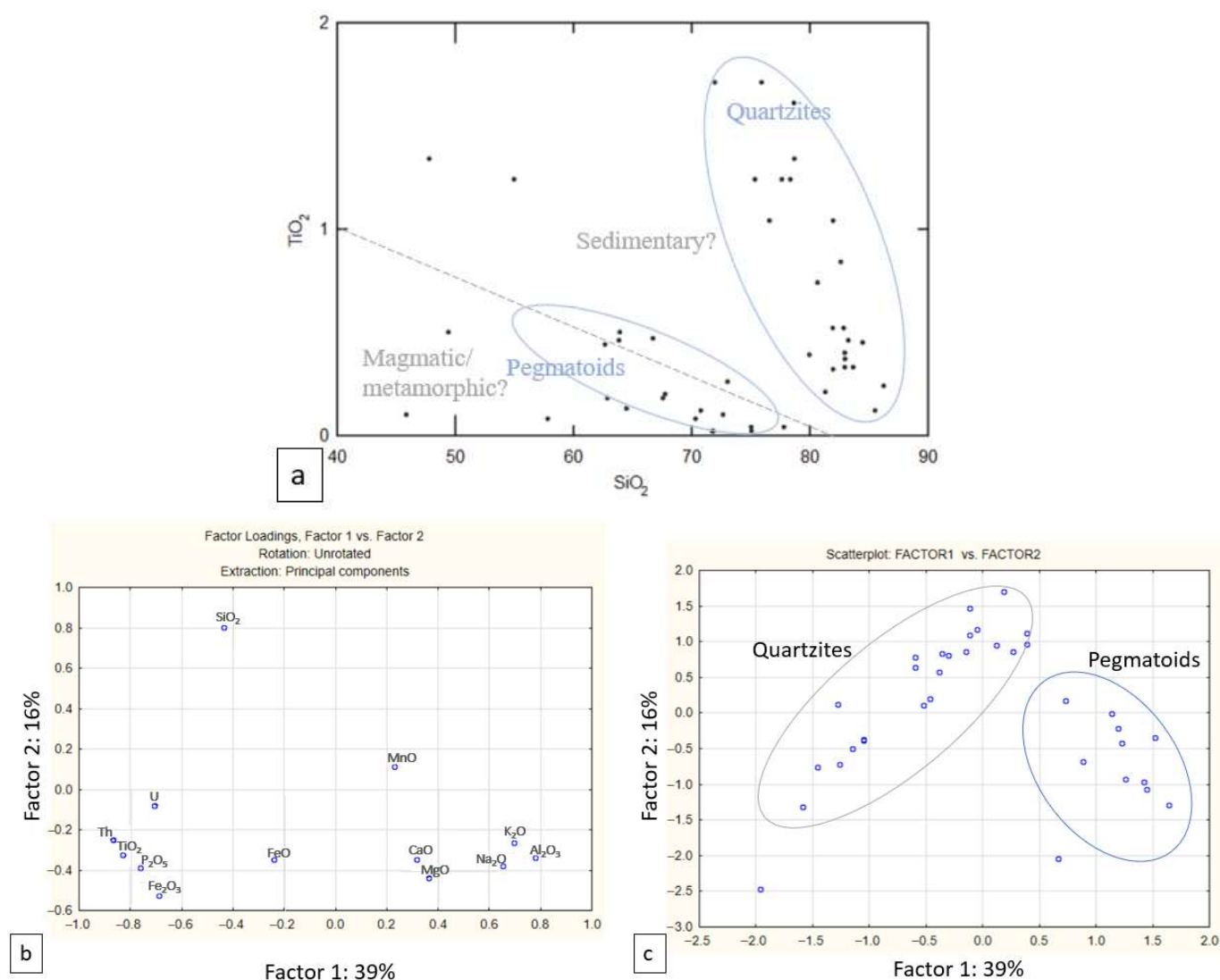


Figure A1. (a) TiO₂ versus SiO₂ (in w%) discrimination diagram (after [35]), showing the quartzites and pegmatoid samples from Dibrova. Line separates sedimentary from igneous protolith (data on graph taken from [13]); (b) projection of the correlation between a variable and a factor of quartzites and pegmatoid samples from Dibrova mineralized zone; (c) projections of individual analyzed points. F1–F2 factor plan.

References

1. Mikhailov, V. *Rare Earth Ores of the World: Geology, Resources, Economics*; Kyiv University: Kyiv, Ukraine, 2010; ISBN 978-966-439-336-9. (In Russian)
2. Zagnitko, V.; Mykhailov, V.; Kryvdic, S.; Sydorhchuk, V. Genetic features and resources of rare metal deposits of the Ukrainian Shield. *Visnyk Geol.* **2017**, *1*, 58–65. (In Ukrainian)
3. Balaram, V. Rare earth elements: A review of applications, occurrence, exploration, analysis, recycling, and environmental impact. *Geosci. Front.* **2019**, *10*, 1285–1303. [CrossRef]
4. Witherly, K. Geophysical expressions of ore systems—Our current understanding. *Soc. Econ. Geol. Inc. Spec. Publ.* **2014**, *18*, 177–208.
5. Goodenough, K.M.; Schilling, J.; Jonsson, E.; Kalvig, P.; Charles, N.; Tuduri, J. Europe's rare earth element resource potential: An overview of REE metallogenetic provinces and their geodynamic setting. *Ore Geol. Rev.* **2016**, *72*, 838–856. [CrossRef]
6. Seamam, J. Rare Earths and China: A Review of Changing Criticality in the New Economy. Notes De L'ifri Ifri, French Institute of International Relations, January 2019. ISSN 978-2-36567-969-5. Available online: <https://www.ifri.org/en/publications/notes-de-lifri/rare-earths-and-china-review-changing-criticality-new-economy> (accessed on 18 July 2023).
7. Kichurchak, V.M.; Bojko, A.Z.; Berzenin, B.Z. About the section of Sachkinska suite of Central-Azov series in the Northern margin of Dibrova structure (Western Azov region). *Geol. J.* **1991**, *4*, 101–107. (In Russian)

8. Sukach, V.; Shpylchak, V.; Hrinchenko, O.; Bondarenko, S.; Isakov, L.; Semka, V. Dibrovskoe deposit - a typical representative of the complex REE-U-Th mineralization in the Azov metallogenic region of the Ukrainian Shield. *Miner. Resour. Ukr.* **2021**, *1*, 18–31. (In Ukrainian)
9. Pokalyuk, V.; Verkhovtsev, V.; Mikhaylichenko, A.; Mikhaylichenko, I.; Zhylyak, E. Dibrovskoe Uranium-Thorium-Rare Earth Ore Occurrence of the Ukrainian Shield (Lithostratigraphic Criteria for the Genesis and Localization of Ore Bodies). *Geochem. Technog.* **2019**, *1*, 57–72. (In Russian) [[CrossRef](#)]
10. Kramar, O.; Wozniak, D.; Nozhenko, O. Peculiarity of the formation and localization rare-earth and uranium-thorium Dibrovskoe deposit of the Ukrainian Shield. In *Prospects for the Development of Uranium Resource Base of Nuclear Power of Ukraine*; Naukova Dumka: Kyiv, Ukraine, 2014; pp. 126–148. (In Ukrainian)
11. Lysenko, A.; Zykov, E.; Falkovich, A.; Kulbachnyi, A. Dibrovskoe rare-earth-thorium-uranium deposit within the Ukrainian Shield. In Proceedings of the Features of the Development of Uranium Mineral Resources of Ukraine, Its Mining and Enrichment Conference, Kiev, Ukraine, 15–17 September 2009; pp. 83–86. (In Russian)
12. Kramar, O. New genetic types of uranium and uranium-thorium mineralization within the Ingul and Azov Megablocks of the Ukrainian Shield. In *Strategic Mineral Resources of Ukraine for Nuclear Energy*; Kulish, E., Ed.; Logos: Kyiv, Ukraine, 2010; pp. 232–267, ISBN 978-966-171-403-7. (In Russian)
13. Semka, V.; Ponomarenko, A.; Bondarenko, S.; Donskoy, N.; Shumlyansky, L.; Melnikova, E.; Semka, L. The Dibrova rare earth-uranium-thorium deposit in the Azov megablock of the Ukrainian Shield. *Geochem. Ore Form.* **2010**, *28*, 48–76. (In Russian)
14. Kalashnik, A.A.; Kuzmin, A.V. Geologicval and structural features of TR-U-Th Dibrovskoe occurrence of the Ukrainian Shield. *Sci. Pap. Sci. Cent. Min. Geol. Geoecol. Infrastructure Dev. Natl. Acad. Sci. Ukr.* **2012**, *10*, 173–185. (In Russian)
15. Osmachko, L. Tectonic conditions of the formation of ore-bearing structures of the Azov Megablock of the Ukrainian Shield (with the example of Dibrovka structure). *Geophys. J.* **2016**, *38*, 113–122. (In Ukrainian)
16. Kramar, O.O.; Kulibaba, V.M. Dibrova Uranium deposit in Azov megablock. Structure, petrology, localization, and genesis. *Collect. Sci. Pap. Inst. Environ. Geochem. Natl. Acad. Sci. Ukr.* **2008**, *16*, 37–50. (In Ukrainian)
17. Vozniak, D.K.; Kramar, O.O.; Bielskyi, V.M. New features of the U-Th-REE genesis of Dibrovskoe deposit in the Pre-Azov megablock. *Collect. Sci. Pap. Inst. Environ. Geochem. Natl. Acad. Sci. Ukr.* **2012**, *20*, 125–129. (In Ukrainian)
18. Shumlyansky, V.O. Thorium mineral resources in Ukraine. In *Institute of Fundamental Research. Scientific Works of the Institute of Fundamental Research*; Shumlyansky, L.V., Ed.; Logos: Kyiv, Ukraine, 2007; ISBN 978-966-581-959-2. (In Russian)
19. Pigulevskiy, P.; Kostenko, N.; Shabatura, O. *The Azov Megablock of the Ukrainian Shield: Tectonics and Substance-Petrophysical Characteristics of Granitoids*; Kyiv University: Kyiv, Ukraine, 2021. (In Ukrainian)
20. Semka, V.; Bondarenko, S.; Stepanyk, L.; Grinchenko, O. Mineralogical -geochemical features and age of thorium-uranium mineralization in Precambrian of the Ukrainian Shield. *Visnyk Taras Shevchenko Natl. Univ. Kyiv Geol.* **2011**, *55*, 24–26. (In Ukrainian)
21. Verkhovtsev, V.; Yuskiv, Y.; Krasov, E. Neotectonics of the territory of Dibrovskoe uranium-rare earth-thorium deposit. *Collect. Sci. Pap. Inst. Environ. Geochem. Natl. Acad. Sci. Ukr.* **2016**, *26*, 156–163. (In Ukrainian)
22. Schulz, B. Monazite Microstructures and Their Interpretation in Petrochronology. *Front. Earth Sci.* **2021**, *9*, 668566:1–668566:22. [[CrossRef](#)]
23. Suzuki, K.; Adachi, M. Precambrian provenance and Silurian metamorphism of the Tsubonosawa paragneiss in the South Kitakami terrane, Northeast Japan, revealed by the chemical Th-U-total Pb isochron ages of monazite, zircon and xenotime. *Geochem. J.* **1991**, *25*, 357–376. [[CrossRef](#)]
24. Montel, J.-M.; Foret, S.; Veschambre, M.; Nicoll, C.; Provost, A. Electron microprobe dating of monazite. *Chem. Geol.* **1996**, *131*, 37–53.
25. Konečný, P.; Kusiak, M.A.; Dunkley, D.J. Improving U-Th-Pb electron microprobe dating using monazite age references. *Chem. Geol.* **2018**, *484*, 22–35. [[CrossRef](#)]
26. Williams, M.L.; Jercinovic, M.J.; Terry, M.P. Age mapping and dating of monazite on the electron microprobe: Deconvoluting multistage tectonic histories. *Geology* **1999**, *27*, 1023–1026. [[CrossRef](#)]
27. Williams, M.L.; Jercinovic, M.J.; Mahan, K.H.; Dumond, G. Electron Microprobe Petrochronology. *Rev. Mineral. Geochem.* **2017**, *83*, 153–182. [[CrossRef](#)]
28. McKechnie, C.L.; Annesley, I.R.; Ansdell, K.M. Radioactive abyssal granitic pegmatites and leucogranites in the Wollaston domain, Northern Saskatchewan, Canada: Mineral compositions and conditions of emplacement in the Fraser Lake area. *Can. Mineral* **2012**, *50*, 1637–1667. [[CrossRef](#)]
29. Suzuki, K.; Kato, T. CHIME dating of monazite, xenotime, zircon and polycrase: Protocol, pitfalls and chemical criterion of possibly discordant age data. *Gondwana Res.* **2008**, *14*, 569–586. [[CrossRef](#)]
30. Săbău, G. Chemical U-Th-Pb geochronology: A precise explicit approximation of the age equation and associated errors. *Geochronometria* **2012**, *39*, 167–179. [[CrossRef](#)]
31. Steele, D.A. Mineral dating using the EPMA: Trials and tribulations. In Proceedings of the Seventh Biennial Symposium. Extended Abstracts, Melbourne, Australia, 18–20 February 2003; p. 78.
32. Bowles, J.F. Age Dating from Electron Microprobe Analyses of U, Th, and Pb: Geological Advantages and Analytical Difficulties. *Misc Microanal* **2015**, *21*, 1114–1122. [[CrossRef](#)] [[PubMed](#)]

33. Li, Z.; Chiro, G.; Bethune, K.M.; Eldursi, K.; Quirt, D.; Ledru, P.; Gudmundson, G. Numerical simulation of strain localization and its relationship to formation of the Sue unconformity-related uranium deposits, eastern Athabasca Basin, Canada. *Ore Geol. Rev.* **2018**, *101*, 17–31. [[CrossRef](#)]
34. Kalashnik, G. The Role of Juvenile Sources of Ore Components in Uranium Ore Genesis of Pryazovye. *Visnyk Taras Shevchenko Natl. Univ. Kyiv Geol.* **2011**, *55*, 53–56. Available online: http://nbuv.gov.ua/UJRN/VKNU_geol_2011_55_18 (accessed on 22 September 2023). (In Ukrainian)
35. Werner, C.D. Saxonian granulites: A contribution to the geochemical diagnosis of original rocks in high-metamorphic complexes. *Gerlands Beitrage zur Geophys.* **1987**, *96*, 271–290.

Disclaimer/Publisher’s Note: The statements, opinions and data contained in all publications are solely those of the individual author(s) and contributor(s) and not of MDPI and/or the editor(s). MDPI and/or the editor(s) disclaim responsibility for any injury to people or property resulting from any ideas, methods, instructions or products referred to in the content.